Small shifts, big ripples: multi-omics studies reveal how ambient temperatures govern Chlamydomonas' cellular responses

Short title: Temperature acclimation in Chlamydomonas

Prateek Shetty,[a,b] Volker Wagner,[a] Dinara Myrzakhmetova,[a] Chia-Chi Peng,[b,c] Chulin Li,[a] Wenshuang Li ,[a,†] Trang Vuong,[a] Joel Ching,[d] Ariane Zander,[d] Rosalind J Allen,[b,d] Markus Lakemeyer,[b,c] Maria Mittag,[a,b,*]

[a] Matthias Schleiden Institute of Genetics, Bioinformatics and Molecular Botany, Friedrich Schiller University, 07743 Jena, Germany

[b] Cluster of Excellence Balance of the Microverse, Friedrich Schiller University, 07743 Jena, Germany

[c] Institute for Organic Chemistry and Macromolecular Chemistry (IOMC), Humboldtstr. 10, Friedrich Schiller University, 07743 Jena

[d] Theoretical Microbial Ecology, Institute of Microbiology, Faculty of Biological Sciences, Friedrich Schiller University, Jena, Germany

[†] Present address: Wuhan Institute of Biomedical Sciences, School of Medicine, Jianghan University, 430056 Wuhan, China

[*] Address correspondence to m.mittag@uni-jena.de

ABSTRACT

Photosynthetic protists known as microalgae face increasing temperatures due to global climate change. The green biflagellate alga *Chlamydomonas reinhardtii* is commonly found in moist soil and serves as a model for investigating these effects. While responses to extreme thermal stress are well characterized, much less is known about the impact of modest, non-extreme temperature shifts. Understanding microalgal responses to subtle temperature changes is critical, as these primary producers drive ecosystem productivity and food web dynamics. Even small shifts may alter algal fitness and reshape interactions with other microbes. Here, *C. reinhardtii* grew at non-stress, ambient temperatures ranging from 18 °C to 33 °C. Transcriptomic profiling revealed extensive reorganization, with over 5,000 transcripts significantly affected, including those involved in algal-bacterial interactions, photoreception, RNA and lipid metabolism, cilia formation, and the secretome. Proteomic analysis of isolated cilia and secreted proteins corroborated these findings, uncovering major changes in abundance within these sub-proteomes, particularly intraflagellar transport (IFT) complexes in cilia and mating-related proteins in the secretome that are both upregulated at higher temperature. Together, these molecular alterations resulted in pronounced changes in growth, cell size, cilia length, swimming behavior, mating ability and bacterial antagonism. These data emphasize major cellular responses upon small temperature shifts.

INTRODUCTION

Chlamydomonas reinhardtii is a unicellular, biflagellate green microalga that lives in moist soil environments (Sasso et al., 2018). The microalga was originally isolated from a potato field in Massachusetts, USA (Harris, 1989). Subsequent studies have repeatedly found members of the genus *Chlamydomonas*, including *C. reinhardtii* in rice paddy soil samples (Barrett and Koch, 1982; Ghasemi et al., 2008; Lin et al., 2013), but also in rice wash water (Szydlowski et al., 2019; Carrasco et al., 2024).

C. reinhardtii, hereafter called Chlamydomonas, is characterized by a single cup-shaped chloroplast, including a pyrenoid along with RUBISCO for carbon dioxide fixation, and a primitive visual system, the eyespot, situated at the edge of the chloroplast near the cell equator (Harris, 1989; Schmidt et al., 2006). Chlamydomonas is a motile alga as it bears two anterior flagella, also called cilia. Each flagellum is anchored by the basal body to the cell. The flagella are structurally and functionally similar to the 9+2-type axonemes of most motile mammalian cilia (Pazour et al., 2005). The flagella contain an intraflagellar transport system (IFT) that is situated between the axoneme and the ciliary membrane and connected with flagellar length control (Marshall and Rosenbaum, 2001). The IFT complex itself is structurally homologous to the mammalian IFT machinery in both composition and functional organization (McCafferty et al., 2022). The ciliary axoneme consists of substructures such as dynein arms and radial spokes that control bending and are essential for motility, mating, and environmental sensing (Marshall, 2024).

The nuclear and organelle genomes of Chlamydomonas are fully sequenced and annotated. In addition, its defined sexual breeding cycle involving plus and minus gametes, along with extensive mutant collections of haploid vegetative cells, allows for genetic crosses and offers precise genetic manipulation using existing toolkits (Merchant et al., 2007; Crozet et al., 2018; Li et al., 2019; Craig et al., 2023). These features have firmly established Chlamydomonas as a model organism for studying a variety of biological processes such as photosynthesis, light perception, cilia biogenesis or synthetic biology (Scaife and Smith 2016; Dupuis and Merchant, 2023).

In recent years, algal-bacterial interactions have come into focus. Algae and bacteria coevolved for hundreds of millions of years, fostering highly relevant ecological associations (Burgunter-Delamare et al., 2024). Chlamydomonas emerged also as a model to study bacterial interactions. Examples include the vitamin B_{12}-based mutualism

(Helliwell et al., 2015; Bunbury et al., 2022) or the antagonism of the bacterium *Pseudomonas protegens* (Aiyar et al., 2017). *P. protegens* secretes toxins including the cyclic lipopeptide orfamide A that deflagellates the cell within a minute by increasing the algal cytosolic Ca^{2+} levels. At least four different algal transient receptor potential channels (TRPs) are involved in mediating the orfamide A signals (Hou et al., 2023).

Temperature is a critical factor in the life of many species. The effects of changes in ambient temperature on microalgal life are, however, poorly understood. Climate warming shifts the species distribution of animals, plants and phytoplankton (Mäkinen et al., 2025) and thus can influence ecosystems. Ambient temperature changes may influence the growth and metabolism of algae, while extreme temperatures may induce stress responses in the short term and lead to cell death in the long term. With climate change driving temperature fluctuations, understanding cellular responses to ambient temperature changes in model algae like Chlamydomonas is essential. Chlamydomonas is conventionally cultivated in the range of 20 °C to 25 °C in the laboratory (Harris, 1989). The alga begins to experience heat stress above 37 °C, marked by the activation of *heat shock protein* (*HSP*) genes, and experiences strong heat stress when the cultivation temperature approaches 43.5 °C (Schroda et al., 2015). A lipidome analysis revealed that Chlamydomonas cells exposed to heat stress of 42 °C exhibited changes in lipid metabolism and increased lipid saturation as an early heat response (Légeret et al., 2016). A recent system-wide analysis made use of transcriptomics and proteomics to study the response of Chlamydomonas to moderate (35 °C) temperature stress that transiently arrests the cell cycle and acute temperature stress (40 °C) disrupting cell division and growth (Zhang et al., 2022). The results showed that some of the responses were shared between the two treatments, although the effects of the 40 °C stress were typically more extensive. For example, both the 35 °C and 40 °C treatments induced starch accumulation, although through distinct mechanisms (Zhang et al., 2022). However, the 35 °C treatment also induced a unique set of responses that were absent at 40 °C. It is also known that low temperatures below 13 °C can induce a cold stress response in Chlamydomonas. Cold stress causes the arrest of cell division, increases the cell size and induces palmelloid formation (Ermilova, 2020). Low temperature adaptation in microalgae also involves production of betaine lipids that are nonphosphorous polar glycerolipids

108 (Murakami et al., 2018) and are specifically found in some microalgae including
109 Chlamydomonas (Riekhof et al., 2005).

110 Most previous studies investigating the effects of temperature on Chlamydomonas
111 have focused on the above-mentioned stress-inducing temperatures. Typically, these
112 studies examine responses to acute heat or cold shock treatments lasting only a few hours
113 to 24 hours, thereby primarily addressing short term acclimation mechanisms. Little is
114 known about how moderate changes in ambient temperature affect the algae when they
115 are grown over several diurnal cycles under these conditions; although some proteins
116 linked with RNA metabolism have been implicated in thermal acclimation (Li et al., 2018).
117 In our present study, Chlamydomonas was maintained under non-stress temperatures
118 ranging from 18 °C to 33 °C for four days, allowing system-wide profiling of its adaptive
119 responses during active growth. This temperature range is particularly relevant because
120 Chlamydomonas is commonly found in moist soils of rice fields, where the temperature
121 typically ranges between 15 °C and 30 °C (Chin et al., 1999). However, with ongoing
122 climate change, soil temperatures are projected to rise, and recent evidence indicates that
123 heat extremes in soil are increasing even faster than air temperature extremes in many
124 regions (García-García et al., 2023). By focusing on non-stress temperatures from 18 °C
125 to 33 °C over several day-night cycles, we sought to investigate how Chlamydomonas
126 might acclimate in the midterm and perform predictions in the longer term where soil
127 temperatures are elevated.

128 Our comprehensive analysis integrates results from multiple assays across four
129 ambient temperatures (18 °C, 23 °C, 28 °C and 33 °C) in Chlamydomonas. Transcriptomic
130 analysis reveals how temperature modulates the expression of transient receptor potential
131 (TRP) channels that are important for some algal-bacterial interactions, components of
132 RNA and betaine lipid metabolism, major photoreceptors, and numerous ciliary and
133 secretome-related transcripts. Based on growth data, we found that effects of increasing
134 temperatures reach a temperature tolerance range at 28 °C. Our transcriptomic results
135 are thus corroborated by immunoblots of selected photoreceptors, analyses of the ciliary
136 and secretory proteomes as well as by behavioral assays performed at 18 °C and 28 °C.
137 Elevated temperatures upregulate many secreted proteins, including those related to
138 mating, resulting in a significant increase in gamete mating efficiency. Furthermore,
139 proteins of the IFT complexes associated with flagellar length control, as well as other key

140 ciliary structural proteins, become more abundant at 28 °C, whereas acetylated tubulin
141 abundance decreases. Importantly, morphological examinations reveal that cell size
142 decreases and cilia length is shortened in cells grown at higher ambient temperatures.
143 Adjustments in ciliary protein composition also affect swimming behavior. At 28 °C, the
144 swimming path of algal cells is characterized by many changes in direction, leading to a
145 reduced speed, while at 18 °C, the cells swim in a linear path without many turns and thus
146 speed up. Together, these results demonstrate that thermal acclimation at different
147 ambient temperatures impacts not only the transcriptome and proteome in
148 Chlamydomonas, but also profoundly influences cell morphology, interspecies
149 interactions, motility, and the sexual cycle.
150

151 **RESULTS**

152 **Ambient temperatures influence the growth and cell size of Chlamydomonas**

153 To address how Chlamydomonas may modulate its physiology and gene expression
154 under non-stressful, ecologically relevant temperature settings, we systematically profiled
155 growth, cell size, and global transcript abundances across a spectrum of ambient
156 temperatures (18 °C, 23 °C, 28 °C, and 33 °C). Cells were grown in a light-dark cycle of
157 12 h light and 12 h dark (LD 12:12) and investigated during the day (see Methods).

158 Our results show that cultivation at 18 °C results in a significantly lower growth rate
159 and reduced final cell density compared to the usual growth temperature of 23 °C, while
160 elevated cultivation temperatures of 28 °C and 33 °C accelerated early growth and
161 achieved greater final biomass (Figure 1A, Supplementary Table 1). The growth limitation
162 at 18 °C becomes evident early in cultivation, with significant differences (compared to
163 growth at the reference temperature of 23 °C) being observed consistently from day 3
164 onwards, ultimately resulting in a significantly reduced final cell density of 1.20×10^7 cells
165 mL^{-1}. In contrast, cultures grown at 28 °C achieved a final cell density of 1.84×10^7 cells
166 mL^{-1}, representing an approximately 20% increase over the 23 °C reference (1.54×10^7
167 cells mL^{-1}). Although the 33 °C cultivation yielded a slightly higher final cell density than
168 the 28 °C cultivation (1.88×10^7 cells mL^{-1} at day 15), cell densities from days 3 to 14 were
169 in most cases higher at 28 °C, indicating that the cells reach their temperature tolerance
170 range around 28 °C (Figure 1A, Supplementary Table 1).

171 We also found that the vertical cell size of the algal cells, measured in the middle
172 of the day at LD6 (Figure 1B), was significantly reduced upon elevation of the cultivation
173 temperature. On day 4, cells grown at 18 °C averaged 8.80 µm in size. Cells cultivated at
174 23 °C exhibited a modest yet significant decrease in mean cell size (to 8.25 µm). Further
175 increasing the temperature to 28 °C and 33 °C intensified this effect, causing the cells to
176 shrink to 6.65 µm at 28 °C and 7.15 µm at 33 °C (Figure 1B, Supplementary Table 2). The
177 observation that temperature-dependent effects are even a bit increased at 28 °C versus
178 33 °C indicates the end of the temperature tolerance range. Similar data were obtained
179 when cell sizes were determined on day 7 for cultures grown at the higher temperatures
180 compared to 18 °C (Supplementary Figure 1).
181 In the next step, we performed comprehensive RNA-seq profiling of cells grown at
182 temperatures of 18 °C, 23 °C, 28 °C, and 33 °C, with three biological replicates at each
183 temperature. Our results revealed marked and temperature-dependent shifts in the global
184 Chlamydomonas transcriptome (Supplementary Table 3). All twelve libraries exceeded 58
185 million raw reads, with ≥62% of trimmed reads aligning to the Chlamydomonas reference
186 genome v6.1. The average mapping rate ranged from ~63% to ~73%. Principal-
187 component analysis (PCA) separated all four temperature conditions along PC1 (50%
188 variance) and PC2 (40% variance), indicating broad transcriptional reprogramming with
189 minimal between-replicate variation (Figure 1C). Together, PC1 and PC2 captured 90%
190 of the total variance. Differential expression analysis highlighted that thousands of
191 transcript abundances were either increased or decreased at elevated temperatures,
192 relative to 18 °C (Figure 1D and 1E). Cultivation at both 28 °C and 33 °C elicited large-
193 scale transcriptional remodeling, with a total of 5,357 and 6,381 genes, respectively, being
194 differentially abundant at a $|\log_2 \text{fold change (FC)}| \geq 1$ and adjusted *P*-value < 0.01.
195 Growth measurements indicated that Chlamydomonas grows better as
196 temperature increases respective to 18 °C, with the optimal growth being at 28 °C and no
197 further gains being observed above this temperature (Figure 1A). Thus, we focused our
198 comparison further on 18 °C vs. 28 °C. The top 1,000 upregulated and the bottom 1,000
199 downregulated genes between the 18 °C and 28 °C samples were identified, and the
200 expression values of these genes were extracted for all four temperature conditions (18
201 °C, 23 °C, 28 °C, 33 °C). This allowed us to construct a comprehensive heatmap revealing
202 distinct expression patterns across the temperature gradient (Figure 1F). These data

203 show that relatively small changes in ambient temperature efficiently remodel the algal
204 transcriptome.

205 Gene ontology enrichment of the transcripts that were differentially abundant
206 between the 18 °C and 28 °C samples revealed several functionally important categories
207 (Figure 1G, Supplementary Table 4). Extracellular matrix (ECM) remodeling emerges as
208 an important theme, with upregulated GO terms including "extracellular region
209 (GO:0005576)" and "polysaccharide catabolic process (GO:0000272)". The
210 Chlamydomonas ECM is composed of pherophorins and other hydroxyproline-rich
211 glycoproteins (HRGPs) and is closely connected to the secretome (Luxmi et al. 2018).
212 Based on these results, it seems that the ECM may undergo modification under different
213 ambient cultivation temperatures. Additionally, flagellar-related GO terms show
214 upregulation at 28 °C, including "dynein complex (GO:0030286)", "ATP hydrolysis activity
215 (GO:0016887)", and "protein tyrosine kinase activity (GO:0004713)". The increased
216 expression of dynein motor proteins and kinase activities suggests enhanced flagellar
217 motor activity. Besides, "ATP hydrolysis activity" is an enriched term, perhaps related to
218 the fact that ciliary motility is driven by dynein motors that hydrolyze ATP (Mitchell et al.,
219 2005). The upregulation of "protein import into peroxisome matrix (GO:0016558)" could
220 indicate altered protein trafficking pathways that may affect flagellar protein assembly.
221 Moreover, protein folding processes including "protein folding (GO:0006457)", "protein
222 refolding (GO:0042026)", and "unfolded protein binding (GO:0051082)" are
223 downregulated at 28 °C.

224

225 **Transcripts encoding photoreceptors and TRP channels show temperature-**
226 **dependent regulation and bacterial antagonism against Chlamydomonas is altered**
227 TRP channels such as the human TRPA1 (Moparthi et al., 2022) or TRP1 of
228 Chlamydomonas (McGoldrick et al., 2019) are known for sensing temperature. Other algal
229 TRPs participate in controlling algal-bacterial interactions, as mentioned before.
230 Transcriptomic profiling identified robust temperature-dependent regulation of transcripts
231 encoding TRP channels (Figure 2A, Supplementary Figure 2). 14 of the 29 known *TRP*s
232 (Hou et al., 2023) are significantly temperature-dependent altered with a $|\log_2 FC| \geq 1$ in
233 their abundances (Supplementary Figure 2). *TRPs 34* and *5* are the most strongly

234 downregulated at 33 °C compared to 18 °C (log_2 fold change close to –11 and –8,
235 respectively). Interestingly, three known TRP transcripts implicated in the orfamide A
236 driven signaling process (*TRP*s 5, 11 and 22; Hou et al., 2023) are altered in their
237 abundance. Besides the *TRP5* channel transcript, *TRP11*, also exhibits significant
238 repression at elevated temperatures, while *TRP22* is slightly enhanced. These changes
239 in the expression of *TRP*s that are involved in orfamide A perception suggest that higher
240 temperatures may alter the vulnerability of Chlamydomonas to orfamide-mediated
241 bacterial attacks. To test if there was any temperature-dependent change of bacterial
242 antagonism, we cocultured Chlamydomonas with *P. protegens* at a ratio of 1:250 in TAP
243 medium at 18 °C, 23 °C, 28 °C and 33 °C. In these cultures, algae are antagonized by the
244 bacteria, as evidenced by visual inspection of the green color of the chlorophyll (Figure
245 2B). We observed that the algal cells in algal-bacterial cocultures cultivated at higher
246 ambient temperatures (either 28 °C or 33 °C) apparently recovered by day 8 of growth in
247 coculture, while they had not recovered by this time at lower ambient temperatures (Figure
248 2B). To track algal cell density more quantitatively, we counted algal cell numbers in
249 monocultures and in cocultures together with *P. protegens*. At 18 °C, Chlamydomonas in
250 coculture with *P. protegens* exhibits reduced growth, with no or little recovery until 11 days
251 (Figure 2C). Similar results are obtained for a coculture grown at 23 °C (Supplementary
252 Figure 3A). In contrast, at 28 °C and 33 °C, algal cells exhibit a much faster recovery in
253 cocultures, resuming growth by day 7 and achieving cell densities closer to those of axenic
254 controls by day 15 (Figure 2D, Supplementary Figure 3B). These findings demonstrate
255 not only that higher ambient temperatures alter TRP-mediated bacterial antagonism but
256 that this also confers real-world protection to Chlamydomonas.

257 Our analysis also revealed temperature-dependent reprogramming of six of the 18
258 known/predicted photoreceptor transcripts (Figure 2E; Greiner et al., 2017; Sharma et al.,
259 2024a). Transcripts encoding channelrhodopsins (CHR1, CHR2), which are located in a
260 specialized part of the plasma membrane covering the eyespot area display pronounced
261 upregulation at higher temperatures. Conversely, two of the four known cryptochrome
262 transcripts, particularly CRY-DASH1, show a strong decrease as the temperature
263 increases. We examined whether the strong up- and down-regulation of the CHR1 and
264 CRY-DASH1 transcripts, respectively, is reflected at the protein level, using immunoblot

265 analyses. In both cases, the protein levels mirrored the tendency found in the transcript
266 profile. Our data reveals a more than fivefold increase in CHR1 protein abundance at
267 28 °C compared to 18 °C (Figure 2F) and a fivefold increase in CRY-DASH1 protein
268 abundance at 18 °C compared to 28 °C (Figure 2G).
269
270 **Ambient temperature drives changes in transcripts encoding proteins of the ciliary**
271 **IFT, the secretory pathway, betaine lipid synthesis and RNA-binding proteins**
272 To further elucidate the molecular adaptations underlying temperature-dependent
273 phenotypic changes in Chlamydomonas, we investigated the expression of additional key
274 gene families highlighted by the gene ontology enrichment, focusing on flagellar
275 assembly, ECM remodeling, RNA-binding proteins and enzymes involved in betaine lipid
276 synthesis.
277 Flagellar trafficking systems, specifically the IFT complexes, are essential for the
278 assembly, maintenance, and function of eukaryotic flagella (Pedersen et al., 2006; Katoh
279 et al., 2016; Ma et al., 2023). The IFT is composed of IFT-A and IFT-B complexes, which
280 coordinate the bidirectional transport of structural and signaling components along the
281 axoneme. Proper IFT activity is fundamental for Chlamydomonas motility, environmental
282 sensing, and cell division. In our transcriptome analysis (Figure 3A), we observed robust
283 and coordinated upregulation of many *IFT-A* and *IFT-B* subunit transcripts in cells grown
284 at both 28 °C and 33 °C compared to 18 °C. These findings, if reflected at the protein
285 level, imply that the upregulation of IFT machinery at higher temperatures reflects a state
286 of active flagellar remodeling.
287 Given the enrichment of ECM-related terms, we next examined changes in
288 transcripts encoding ECM proteins. The ECM in Chlamydomonad algae such as *Volvox*
289 *carteri* is primarily composed of hydroxyproline-rich glycoproteins, particularly
290 pherophorins and related structural proteins. Phylogenetic analyses comparing *V. carteri*
291 and Chlamydomonas have revealed that both species possess numerous pherophorin-
292 related proteins. In *V. carteri*, 74 of 99 of these proteins are species-specific, while in
293 Chlamydomonas, 10 of 30 are unique to the species (von der Heyde and Hallmann, 2022).
294 These ECM components play a pivotal role in maintaining cell wall integrity, protection,
295 signaling, and morphogenesis. They not only provide mechanical stability but also
296 participate in cell-cell communication and environmental adaptation (Hallmann, 2006).

297 Matrix metalloproteases (MMPs) are key regulators of ECM remodeling, cleaving
298 glycoproteins to facilitate matrix turnover and structural adaptation. Both are tightly
299 connected to the algal secretome (Luxmi et al., 2018). Our data show consistent and
300 dramatic downregulation of multiple transcripts encoding ECM proteins and MMPs at
301 higher temperatures (Figure 3B).

302 We also addressed betaine lipid synthesis that is known to be involved in abiotic
303 stresses, including cold temperatures (Salomon et al., 2025). We found that three
304 transcripts encoding enzymes involved in the betaine lipid (known as diacylglyceryl-N, N,
305 N-trimethylhomoserine) pathway are significantly downregulated at the lower ambient
306 temperature of 18 °C compared to 28 °C (Figure 3C). These include *S-*
307 *adenosylmethionine synthetase1* (*SAS1*), the consequently acting *S-adenosyl-L-*
308 *methionine decarboxylase* (*SAMDC*) and the *betaine lipid synthase* (*BTA1*, Figure 3E).
309 These data highlight that betaine lipid synthesis is already affected at lower ambient
310 temperature compared to cold stress, at least at the transcript level.

311 Finally, we screened RNA-binding proteins (RBPs), which tune gene expression
312 post-transcriptionally or translationally. Nine transcripts encoding RBPs are responsive to
313 ambient temperatures (Figure 3D). Some RBP transcripts, encoding Pumilio or Musashi
314 proteins, are mostly significantly upregulated higher temperatures, while the C3 and C1
315 subunit transcripts of the RNA-binding protein CHLAMY1 (*CRB1* and *CRB3*; Zhao et al.,
316 2004) as well as NAB1 and DUS16 are downregulated at higher temperatures. Some of
317 these data are reflected at the protein level, as discussed later.

318

319 **Temperature-dependent remodeling of the flagellar proteome results in shorter**
320 **flagella in cells grown at 28 °C**

321 Transcriptome analysis revealed that many transcripts encoding ciliary IFT proteins are
322 altered in their abundances in cells grown at 18 °C compared to 28 °C (Figure 3A). To
323 examine whether these changes are reflected at the protein level, we performed label-
324 free quantitative proteomic analyses on the membrane-matrix-axoneme (MMA) fraction of
325 purified flagella from cells grown at 18 °C or 28 °C (see Methods) using single-pot phase-
326 enhanced sample preparation (Hughes et al., 2019) and liquid chromatography
327 electrospray ionization tandem mass spectrometry (LC-ESI-MS/MS, see Methods). We
328 identified a total of 3,271 proteins with at least two unique peptides (Supplementary Table

329 6). We generated a high-confidence ciliary protein list by matching all detected proteins
330 against the Chlamydomonas ciliary protein database established by Pazour et al., 2005
331 (https://chlamyfp.org/ChlamyFPv2/cr_read_sql.php). This comparison yielded 1,395
332 overlapping proteins, which we defined as the high-confidence ciliary MMA proteome
333 (Supplementary Table 7). All subsequent differential abundance analyses were restricted
334 to this set of 1,395 proteins. Using a differential abundance threshold of $|\log_2 FC| \geq 0.5$ and
335 adjusted *P*-value < 0.05, we identified 144 ciliary proteins as significantly upregulated and
336 47 as significantly downregulated at 28 °C compared to 18 °C (Figure 4A, Supplementary
337 Table 8). Most notably, there was a strong and coordinated upregulation of the IFT-
338 machinery: five of six IFT-A subunits and three of the 16 IFT-B subunits significantly
339 increased in abundance (Figure 4B). This proteomic signature mirrors some of the
340 transcript levels (*IFT*s 121 and 120 of complex A and *IFT*s 74 and 81 of complex B)
341 elevated at 28 °C (Figure 3A). It should be, however, noted that all other transcript levels
342 belonging to the upregulated IFT proteins (*IFT*s 43, 139, 144 of the IFT-A complex and
343 *IFT*-B 80) are also significantly upregulated in cells grown at 28 °C, but with a $|\log_2 FC|$ of
344 less than 1 (Supplementary Table 3).

345 It is known that Chlamydomonas can alter flagella length by activating axonemal
346 disassembly and stimulating IFT trafficking (Marshall and Rosenbaum 2001; Pan and
347 Snell, 2005). To determine whether the observed protein trends translate into a
348 morphological phenotype, we performed immunolocalization of cilia using anti-acetylated
349 tubulin antibodies (Figure 4C). On day 4 of growth, flagellar length was the longest in cells
350 cultivated at 18 °C, reaching a mean flagellar length of 8.50 µm under the growth
351 conditions that were used at LD6 (see Methods). As the cultivation temperature increased,
352 flagellar length progressively reduced, reaching an average of 6.14 µm at 28 °C and 6.03
353 µm at 33 °C (Figure 4D, Supplementary Table 9). Comparable results were observed on
354 day 7 of growth at LD6 (Supplementary Figure 4, Supplementary Table 9).

355 We also verified whether the reduction in cilia length is reflected in the amount of
356 the major ciliary tubulin, being α-tubulin1. We observed a small but non-significant
357 decrease in α-tubulin 1 abundance comparing its level in cells grown at 18 °C versus 28
358 °C, as measured by LC-ESI-MS/MS (Figure 4E, upper part). However, flagellar α-tubulin
359 differs from cell body α-tubulin, as it gets post-translationally modified by acetylation

360 (L'Hernault and Rosenbaum, 1985). To verify the amount of α-tubulin in the flagella, we
361 performed immunoblots with flagellar proteins along with anti-acetylated tubulin
362 antibodies. As loading control and for comparison, we used antibodies against casein
363 kinase 1 (CK1) that is slightly increased in cells grown at 28 °C. The immunoblot analyses
364 showed a clear reduction of acetylated tubulin while CK1 levels were enhanced in cells
365 grown at 28 °C (Figure 4E, lower parts; Supplementary Figure 5). These data corroborate
366 the length reduction of the cilia along with their axoneme.
367

368 **Temperature-driven changes in flagellar proteins connected to motility alter algal**
369 **motility patterns**

370 Further analysis of the flagellar proteome revealed substantial temperature-dependent
371 remodeling of Chlamydomonas' motility machinery (Figure 5A). A plethora of major motor
372 proteins, including axonemal and cytoplasmic dynein heavy chains, kinesin motor proteins,
373 and dynein light/intermediate chains, exhibited pronounced upregulation at 28 °C,
374 suggesting a heightened demand for active transport and mechanical work within the
375 flagellum at elevated temperatures. Similarly, proteins associated with ciliopathy
376 syndromes, especially the Bardet–Biedl syndrome (BBS) proteins, showed strong
377 upregulation at 28 °C. BBS proteins are connected to IFT trains and influence phototactic
378 behavior (Liu and Lechtreck, 2018). In contrast, ankyrin repeat proteins (FAP164 and
379 FAP208), which are critical for maintaining axonemal stability and regulating ciliary and
380 flagellar architecture, displayed reduced abundance. Moreover, downregulation of two
381 zinc chaperones (ZNG1, ZNG2) was observed in cells grown at 28 °C. A similar trend was
382 detected in the GO enrichment analyses, since protein folding and protein refolding were
383 enriched GO terms, with many transcripts showing downregulation at 28 °C (Figure 1G).
384 Such chaperones are important for maintaining protein homeostasis and might play a role
385 in flagellar assembly under changing environmental conditions, also at lower temperature.
386 We also sought to investigate the possible behavioral consequences of these
387 molecular changes in flagellar related proteins, by taking a close look at cell motility. For
388 this purpose, we examined the motility of Chlamydomonas cells using microscopy in a
389 temperature-controlled chamber, combined with the ImageJ plugin TrackMate (see
390 Methods), which quantifies various parameters associated with cell trajectories, including
391 average speed and the turning angle, indicating to what extent cells change their direction

392 between frames. For this purpose, we used the same cell densities for all samples (see
393 Methods and Discussion). Representative trajectories for individual cells grown at each
394 temperature illustrate severe shifts in motility patterns. Many cells grown at 18 °C followed
395 relatively straight paths, with infrequent directional changes (Figure 5B, Video 1). In
396 contrast, many cells grown at 28 °C exhibited more constrained paths characterized by
397 frequent apparent abrupt directional changes (Figure 5C, Video 2). Figure 5B and C show
398 the trajectories of the individual cells for 80 s, the videos show six exemplarily tracked
399 cells for a total of 57 s. Quantitative analysis of over 150 tracked cells per biological
400 replicate confirmed these observations. It should be noted that the basic swimming
401 behavior of Chlamydomonas involves helical movement with breaststrokes when moving
402 forward (Crockett, 2021). This ensures that the eyespot situated at the nearby *cis*-
403 flagellum perceives light from all directions. The directional change between frames,
404 averaged over a trajectory, was significantly higher in cells grown at 28 °C (Figure 5D).
405 We also calculated the mean swimming speed along each trajectory. Averaging over
406 trajectories, this was significantly reduced in cells cultivated at 28 °C (Figure 5E),
407 consistent with the concept that frequent course corrections lead to slower cell speed.
408 Taken together, the proteome from cells grown at 28 °C reveals more dynamic
409 flagella with heightened intraflagellar transport, increased abundance of axonemal motors
410 and motility patterns that favor exploratory turning, compared to the more linear swimming
411 that occurs at 18 °C.
412

413 **Temperature-driven changes in the Chlamydomonas secretome and consequences**
414 **for mating efficiency**

415 Transcriptomic analyses revealed pronounced downregulation of transcripts encoding
416 ECM components, specifically the pherophorins and MMPs, that are all linked to the
417 secretome (Luxmi et al., 2018). Thus, in the next step, we analyzed whether the
418 Chlamydomonas secretome also changed with cultivation temperature, using label-free
419 quantitative proteomics (see Methods). Mass-spectrometric profiling of Chlamydomonas
420 proteins in supernatants (see Methods) of cells cultured at 18 °C and 28 °C identified a
421 total of 2,763 proteins with at least two identified peptides (Supplementary Table 10). We
422 analyzed these 2,763 proteins using DeepLoc to predict extracellular proteins. Of the
423 2,763 proteins detected, 557 were predicted by the program as extracellular proteins and

424 constituted our final dataset of secreted proteins (Supplementary Table 11). Using
425 thresholds of $|\log_2 FC| \geq 0.5$ and adjusted *P*-value < 0.05, we found that 317 proteins were
426 significantly upregulated and 49 were significantly downregulated at 28 °C relative to
427 18 °C (Figure 6A, Supplementary Table 12).

428 While many proteins of the cilia coincide in their transcript and protein abundances,
429 the secretome responds in the opposite direction to the transcriptome. Many transcripts
430 encoding ECM proteins and other secretory proteins are downregulated (Figure 3C) or
431 unchanged, but a large number of secreted HRGPs, pherophorins and MMPs is strongly
432 upregulated in cells grown at 28 °C relative to 18 °C (Figure 6B). We also compared the
433 ambient temperature-altered secretomes against the published Chlamydomonas mating
434 secretome, measured at 22 °C (Luxmi et al., 2018), and identified interesting overlaps
435 between the two datasets. The ambient temperature-altered secretome contains
436 numerous proteins with established roles in mating, including multiple pherophorins,
437 gametolysins, and subtilisin-like proteases (these are all marked with a * in front of the
438 name in Figure 6B). The differential regulation of VLE1, a key subtilisin-like protease that
439 is also released during gametogenesis, was particularly relevant, as discussed later. The
440 temperature-dependent regulation of gametogenesis-related proteins could prime cells for
441 developmental programs that are advantageous under warmer conditions, potentially
442 accelerating the onset of mating competence.

443 To test this hypothesis functionally, we performed mating experiments using
444 Chlamydomonas strains CC-124 (mt^+) and CC-125 (mt^-), routinely used for mating assays
445 in our laboratory (Müller et al., 2017). Strains were cultivated under nitrogen-limited
446 conditions at different ambient temperatures (see Methods). Mating efficiency assays
447 confirmed that higher cultivation temperatures significantly increase gamete fusion
448 success, with cultures pre-conditioned at 28 °C showing enhanced mating competency
449 compared to those grown at 18 °C (Figure 6C).

450

451 **DISCUSSION**

452 We used transcriptome analysis to uncover gene expression changes in the biflagellate
453 model microalga Chlamydomonas acclimated to different ambient temperatures. We
454 complemented these data with proteomic and behavioral analyses that highlighted

455 structural changes in cilia impacting the swimming trajectories and speed. We observed
456 shifts in algal-bacterial interactions, photoreceptor regulation, and marked changes in the
457 secretome, connected to enhanced mating behavior, at higher temperatures. The
458 temperature ranges investigated included 18 °C, 23 °C, 28 °C, and 33 °C for
459 transcriptomic analyses, while our proteomic analyses focused on 18 °C and 28 °C. These
460 conditions differed from those in previous system-level studies, which primarily addressed
461 moderate or acute heat stress at 35 °C and 40 °C, compared to normal (25 °C) and heat-
462 stressed growth (Zhang et al., 2022; Zhang et al., 2024), or examined cold stress below
463 15 °C (Valledor et al., 2013). Anticipating that climate change will both shift the typical
464 range of temperatures and increase extreme stress situations, it is central to understand
465 cellular responses over both stress-inducing and ambient temperature ranges. In their
466 natural habitat of rice fields, Chlamydomonas has historically been exposed to
467 temperatures ranging from 15 °C to 30 °C (Chin et al., 1999). In this study, a range of
468 temperatures extending 3 °C beyond the natural limits experienced by Chlamydomonas
469 were tested, allowing us to investigate the effects of moderate warming without exposing
470 the algae to heat stress. Our results show that growth rates at 28 °C and 33 °C were
471 similar, as seen in Figure 1A, indicating that maximum growth is achieved at 28 °C.
472 Current temperature measurements in a flooded sandy rice soil field in Italy (dated June
473 20, 2025) revealed an external temperature of 35 °C, with soil temperature of 30 °C at 0
474 cm and 25 °C at 10 cm depth during the day (data put in order with Innovatech Agro, Italy).
475 Thus, our studies capture actual relevant changes.

476 The transcriptome studies performed with cells grown in the range between 18 °C
477 and 33 °C revealed changes in the abundances of more than 5,000 and 6,000 transcripts,
478 respectively, between 18 °C and 28 °C (or 33 °C), covering roughly one third of all
479 transcripts based on the genome vs 6.1 (Craig et al., 2023). These data highlight that
480 ambient temperature changes remodel the algal transcriptome drastically.

481 While missing in land plants, animals and some algae have a high number of TRP
482 channels (Verret et al., 2010). 14 of the 29 annotated TRP channel transcripts based on
483 vs 6.1 of the Chlamydomonas genome (Hou et al., 2023) are significantly altered by
484 temperature with a $|\log_2 FC| \geq 1$. Especially interesting findings include the changes in
485 transcript abundances encoding the TRP channels 5, 11 and 22 that are involved in the
486 antagonistic interaction of the bacterium *P. protegens* against Chlamydomonas (Hou et

487 al., 2023). These three channels group close to the vanilloid family (TRPV) tree that
488 includes thermosensitive and calcium-permeable members in mammals, playing also a
489 role in autoimmune diseases (Xiao et al., 2025). Among them, the *TRP5* transcript is most
490 strongly downregulated in cells grown at 33 °C, but also shows a significant decrease at
491 28 °C. *TRP5* transcript abundance also decreases, in conjunction with a thickening of the
492 algal cell wall, when algal cells are transferred to 3-dimensional (3-D) conditions in the
493 presence of acetate to simulate nature-like conditions in rice fields (Vuong et al., 2025).
494 Since algal fitness against antagonistic bacteria is enhanced under 3-D conditions, we
495 analyzed whether ambient temperature changes would similarly influence algal-bacterial
496 antagonism. We show that higher ambient temperatures indeed enhance algal fitness
497 (Figure 2B - D, Supplementary Figure 3). This may be due to a combination of events
498 happening at higher temperatures, including the decrease of two involved TRP channel
499 transcripts, *TRP5* and *TRP11*. Based on our prior studies (Hou et al., 2023), we assume
500 that the strong decrease of these two channels versus the slight increase of *TRP22* at the
501 higher temperatures will result in a reduced deflagellation rate upon orfamide A exposure
502 and thus strengthen algal fitness. But enhanced algal fitness may be also related to the
503 increased ECM particles found at the higher temperature as shown in the secretome study
504 (Figure 6B). The strongest altered *TRP* transcript (Supplementary Figure 2) was *TRP34*
505 encoding also a member that groups closely to the TRPV family (Hou et al., 2023). In
506 contrast, *TRP1* of Chlamydomonas whose heterologous expression and purification
507 revealed the opening of the pore channel in response to a temperature of 28 °C or 29 °C
508 (McGoldrick et al., 2019), groups closest to the TRP family of yeast and fungi (TRPY/F,
509 Hou et al., 2023). *TRP1* was found to be significantly upregulated at 28 °C in our
510 transcriptome study, however, with a $\log_2$ FC of less than 1 (Supplementary Table 3).
511 18 known/predicted photoreceptors are encoded in the genome of
512 Chlamydomonas (Greiner et al., 2017; Sharma et al., 2024a). Transcriptome analyses
513 revealed that transcripts encoding six of these photoreceptors are regulated by ambient
514 temperature changes. For two photoreceptors, CHR1 and CRY-DASH1, changes in
515 transcript abundance were also studied at the protein level; while CHR1 is being
516 upregulated at 28 °C, CRY-DASH1 is downregulated at 28 °C (Figure 2F and 2G). In land
517 plants, it was shown that photoreceptors sense stress based as well as ambient
518 temperature changes (reviewed in Sharma et al., 2024b). Our data emphasizes that algal

519 photoreceptors can also sense ambient temperature variations. Moreover, CHR1, a
520 microbial channelrhodopsin emerged as a major tool in modern biological research and
521 was one of the first algal photoreceptors used for optogenetic approaches (Deisseroth
522 and Hegemann, 2017; Christie and Zurbriggen, 2021). In the algal cell, CHR1 is involved
523 in phototactic behavior and is situated in a specialized part of the plasma membrane
524 surrounding the eyespot (Schmidt et al., 2006). Variations in CHR1 abundance could
525 contribute to the altered motility pattern observed at higher temperatures, where algal cells
526 displayed more frequent turns (Figure 5 D and E). The other photoreceptor, CRY-DASH1,
527 helps balance the photosynthetic machinery by acting as a negative regulator that
528 prevents hyper-stacking of thylakoid membranes (Rredhi et al., 2021). In addition, it is
529 involved as a positive regulator in anoxic metabolism (Rredhi et al., 2024). Our data
530 indicates that these processes may be changed in a temperature-dependent way,
531 although this relationship requires further investigation.

532 As many transcripts involved in the ciliary structure and in the cellular secretory
533 processes were modified at different temperatures, we extended our studies to include
534 the ciliary and secretory sub-proteomes. Proteomic analysis of the ciliary MMA fraction
535 isolated from cells grown at 18 °C and 28 °C, respectively, revealed a strong increase of
536 most IFT-A and some IFT-B complex proteins, which are crucial for intraflagellar transport
537 from the base of the cilia up to the tip (anterograde IFT train) and from the tip down to the
538 basal body (retrograde IFT train) (Lacey et al., 2024). The increase in IFTs observed at
539 the transcriptome and protein levels (Figures 3A and 4B, Supplementary Table 3)
540 coincides with the upregulation of many motor proteins such as kinesin II motor proteins
541 FLA8, FLA10 and KAP1 (FLA3) and several dyneins (Figure 5A) at higher temperature
542 while the post-translationally modified acetylated α-tubulin is downregulated under these
543 conditions (Figure 4E). The remodeling of many ciliary protein abundances, including the
544 reduced α-tubulin levels in cells grown at 28 °C correlates with shorter cilia observed at
545 this temperature in the middle of the day (LD6, Figure 4C and D). The control of flagellar
546 length in Chlamydomonas is related to the diurnal cycle (Tuxhorn et al., 1998) and is linked
547 with IFT particles as well as axonemal disassembly. This process has been discussed in
548 various models (Marshall & Rosenbaum, 2001; Pan and Snell, 2005; Wemmer et al., 2020;
549 Patel et al., 2024). Moreover, five proteins of the BBS complex (BBS-2, -4, -7-, -8 and -9)
550 related to ciliopathies are increased in abundance in cells grown at 28 °C (Figure 5A).

551 Previous studies found that a purified BBS-like complex containing BBS1, -4, -5, -7, -8
552 associate with a subset of IFT proteins (Lechtreck et al., 2009). Three of these IFT-
553 associated BBS proteins are also temperature-regulated. Interestingly, some
554 Chlamydomonas BBSome mutants (*bbs1*, *bbs4*, *bbs7*), can assemble full-length, motile
555 flagella but become completely non-phototactic, due to an unregulated accumulation of
556 critical signaling proteins (Lechtreck et al., 2009). These results may thus also connect
557 with the observed modified swimming behavior at 18 °C and 28 °C (Figure 5 B-E).
558 Behavioral changes in swimming trajectories have been found before under cold and heat
559 stress conditions; they depend further on the acclimation duration (Meier et al., 2022). In
560 addition to temperature and acclimation, population density plays an important role in the
561 determination of swimming speed. The speed increases with higher cell densities due to
562 the secretion of a low-molecular weight compound (Folcik et al., 2020). Here we used the
563 same cell density for all measurements and kept it relatively low (5×10^5 cells mL^{-1}) for
564 comparative studies. This density was selected due to the limited growth of cultures at
565 18 °C by day 4 after inoculation (Figure 1A, Methods). The calculated speeds are in the
566 range of priorly observed speeds of Chlamydomonas cells based on similar cell numbers
567 (Folcik et al., 2020). Using a specialized temperature-controlled microscopy setup (see
568 Methods), we revealed that even ambient changes in temperature result in severe
569 alterations in swimming speed as well as in the frequency of turns performed by the algal
570 cells.

571 The analysis of the secreted proteome revealed a striking temperature-dependent
572 reorganization in Chlamydomonas characterized by the substantial upregulation of MMPs,
573 the vegetative lytic enzyme1, VLE1, and a diverse array of pherophorins at 28 °C, creating
574 a molecular environment primed for extensive ECM modification. MMPs belong to a family
575 of zinc-dependent proteinases and can cleave diverse substrates including components
576 of the ECM (Hey and Linder, 2024). One of the first MMPs of Chlamydomonas that was
577 characterized represents the gamete lytic enzyme (Kinoshita et al., 1992), but several
578 MMPs and other proteolytic enzymes such as VLE1 have been also found in the mating
579 secretome performed at 22 °C (Luxmi et al., 2018). Pherophorins are a major group of
580 extracellular hydroxyproline-rich proteins in Chlamydomonas (Barolo et al., 2022) and are
581 also important in *V. carteri* in ECM biosynthesis (von der Heyde and Hallmann, 2022). 18
582 pherophorins are upregulated at higher temperature as well as eight further

583 hydroxyproline rich proteins, including CWP2, FAPs 40, 113 and 137, ISGs 2 and 6,
584 MAW4 and VSP3. Several of these proteins (marked by an asterisk in Figure 6B) overlap
585 with proteins identified in the Chlamydomonas mating secretome study (Luxmi et al.,
586 2018). Sexual algal reproduction was shown earlier to depend on the secreted protein
587 profile (Snell et al., 1989). Our results highlight that cultivation at elevated ambient
588 temperatures significantly enhances the secretion of proteins required for mating. Thus,
589 we examined the mating efficiency of plus and minus gametes at different temperatures
590 and found that gametogenesis increases as temperature rises (Figure 6C). These data
591 highlight a direct influence of small ambient temperature changes on the sexual life cycle
592 of Chlamydomonas.

593 The ciliary and secretome proteomes identified more proteins (Supplementary
594 Tables 6 and 10) than are present in the ciliary database (Supplementary Table 7) and
595 predicted to be localized extracellularly by DeepLoc (Supplementary Table 11),
596 respectively. We are aware that these proteins may be contaminants. For example, at
597 higher temperature, some cells may have been subject to cell lysis and thus may have
598 influenced the results. It may, however, also be the case that some candidates have been
599 neglected based on the selection criteria used. For example, VLE1 is well known as
600 secreted protein (Luxmi et al, 2018), but it is not predicted to be localized to the
601 extracellular region with DeepLoc. Due to the prior study, it has been included in our list.

602 In some cases, the transcriptome changes agree with changes found at the protein
603 level, but in other cases, especially with the secretome, correlations are scarce or even
604 contradictory. Thus, post-transcriptional and translational control mechanisms along with
605 RBPs are most likely involved. The transcriptome studies have shown that transcripts
606 encoding a variety of RBPs are altered (Figure 3D). Former studies of RBPs selected at
607 different ambient temperatures had revealed that the C3 subunit of RBP CHLAMY1
608 (CRB3) is downregulated at the protein level in cells grown at 28 °C compared to 18 °C
609 (Li et al., 2018), which agrees with its transcript level (Figure 3D). Notably, the C3 subunit
610 confers thermal acclimation to Chlamydomonas as shown by mutant lines (Li et al., 2018).

611 Our present studies highlight that temperature acclimation to different ambient
612 temperatures represents an important step in the regulation of a variety of biological
613 processes in Chlamydomonas. Some of the depicted components such as TRP channels
614 and photoreceptors are likely to be members of the thermal acclimation pathway involved

615 in sensing ambient temperatures. Components like the C3 subunit seem to mediate
616 sensed information. Finally, there are several members like IFT or ECM proteins involved
617 in executing cellular responses like the shortening of the cilia or the enhancement of
618 protein secretion. These events then induce behavioral changes such as swimming speed
619 and turns, mating ability or bacterial antagonism. Altogether, our findings show that even
620 modest changes in temperature, that may seem negligible at first glance, influence key
621 properties of the organism and demand further focused study in the future. Thus, small
622 shifts can indeed cause big ripples.
623

624 **METHODS**

625 **Strains of *Chlamydomonas reinhardtii* (thereafter Chlamydomonas) used and**
626 **quantification of growth**

627 Chlamydomonas wild-type strain SAG 73.72 (mt^+) was obtained from the Culture
628 Collection of Algae at Göttingen University and used for all experiments except for the
629 mating assay. Strain SAG73.72 is an isolate of Tsubo's strain C8 that is close to 21 gr
630 from Sager (Harris, 1989). Strain 21 gr served as a crossing partner for generating strain
631 CC-4532, whose genome has been sequenced (Craig et al., 2023).

632 Cells were cultivated in Tris-Acetate-Phosphate (TAP) medium (Harris, 1989)
633 under a 12h : 12h light:dark (LD) cycle at a light intensity of 50 µmol m^{-2} s^{-1} and stirring
634 (100 rpm). Growth experiments were performed under four cultivation
635 temperatures,18 °C, 23 °C, 28 °C, and 33 °C. To initiate precultures, cells were transferred
636 from TAP agar plates (Harris 1989) into 15 mL of liquid TAP medium in sterile NUNC
637 flasks. These were incubated at the designated temperatures with orbital shaking at
638 100 rpm under the LD cycle for 4 days. On day 4, main cultures were prepared by
639 measuring the cell density of each preculture and adjusting the starting concentration to
640 1×10^5 cells mL^{-1}. This step ensured uniform inoculum density across all temperature
641 conditions. Culture densities were quantified daily by sampling 180 µL of sample and
642 counting cells on an improved Neubauer chamber (no. T729.1; Carl Roth, Karlsruhe,
643 Germany). Visual documentation of chlorophyll content (as a proxy for pigmentation and
644 viability) was also captured every second day by photographing culture flasks. Cell
645 samples for the different experiments were always taken in the middle of the day, at LD6,
646 unless otherwise indicated.

647

648 **Determination of cell size**

649 Cell sizes were quantified on day 4 and day 7 of growth (Figure 1A). For this purpose, 2
650 mL aliquots from the main Chlamydomonas cultures were harvested and centrifuged at
651 500 *g* for 10 min. The algal cells were fixed with Lugol's solution and further treated as
652 described previously (Vuong et al., 2025). Brightfield microscopy images along with a
653 Zeiss Axiophot were taken to measure multiple cells with ImageJ (version 1.53t, Schneider
654 et al., 2012) taking the vertical length of the cells into consideration.

655

656 **Transcriptome sequencing and data analysis**

657 Total RNA was isolated from cells grown in TAP media under four different ambient
658 temperatures, with three biological replicates per condition. Total RNA was extracted
659 using the Qiagen Plant RNeasy Mini kit (Qiagen, Germany) according to the
660 manufacturer's instructions. RNA concentration and purity were measured using a
661 NanoDrop ND-1000 UV/Vis spectrophotometer (Thermo FisherScientific, USA). Library
662 preparation and sequencing were performed by Eurofins Genomics (Ebersberg,
663 Germany). For each sample, stranded TruSeq cDNA libraries were prepared using
664 poly(A) enrichment. Libraries were sequenced on an Illumina NovaSeq 5000 platform to
665 generate 150 bp paired-end (PE) reads. The raw reads were processed using Fastp
666 (v.0.23.4) (Chen et al., 2018) with default trimming options and base correction enabled
667 to correct for low-quality bases. Kallisto (v0.50.1) (Bray et al., 2016) was used to quantify
668 the abundance of each transcript against the reference *C. reinhardtii* v.6.1 transcriptome
669 downloaded from Phytozome. All further analysis was carried out in Rstudio (v.2024.04.1,
670 Posit team, 2023). R tximport package (v.1.32.0) (Soneson et al., 2015) was used to
671 import the gene-level expression and normalize the data. Genes with read counts fewer
672 than 10 reads in at least 6 samples were marked as lowly expressed and removed from
673 further analysis. Differential expression analysis was carried out using DESeq2 package
674 (v.1.44.0) (Love et al., 2014). A gene was considered statistically significant if the $|\log_2$
675 (fold change)| was ≥ 1 and the adjusted *P*-value < 0.01. Cultures grown at 18 °C served as
676 the reference condition for all pairwise comparisons. Genes with positive $\log_2$ fold changes
677 were designated as upregulated, and those with negative values were designated as

678 downregulated relative to the 18 °C condition. Gene ontology enrichment was carried out
679 using topGO (v.2.56.0).
680
681 **Isolation of flagella and ciliary proteins from the membrane-matrix-axoneme (MMA)**
682 **fraction**
683 Cells were grown under the above-mentioned conditions for four days at 18 °C and 28 °C,
684 respectively. Cells were harvested and washed according to Bösger et al. (2014). The
685 temperature of rotors and washing buffers was adjusted to 18 °C and 28 °C, respectively.
686 After deflagellation of the cells with dibucain and purification of the flagella using sucrose
687 step-gradient centrifugation, the MMA fraction was prepared by adding NP-40 to the
688 isolated flagella to achieve a final concentration of 1%, as described in Bösger et al. (2014).
689 Four independent biological replicates were prepared for each temperature condition,
690 from which three were used for further analysis.
691
692 **Proteome analysis of the MMA fraction**
693 For the analysis of the proteins in the MMA fraction, 0.5 mg proteins of each MMA fraction
694 were reduced and carbamidomethylated according to Zhang et al., 2005. Samples were
695 then subjected to the single-pot, solid phase-enhanced sample preparation (SP3)
696 according to Hughes et al., (2019). Briefly, the proteins were bound to magnetic SP3
697 beads, washed three times to remove contaminants, and digested overnight at 37 °C
698 directly on the beads by adding 20 µg of a Trypsin and LysC protease mix (MS grade,
699 Promega V507A) dissolved in 40 µL of the provided buffer per 0.5 mg sample in Eppendorf
700 Protein LoBind tubes that were shaken at 1,000 rpm in a Thermomixer. Prior to the mass
701 spectrometric analyses, the resulting peptides were further purified by reversed phase
702 chromatography using ZipTip microtips supplemented with additional Poros R2 10 µm
703 reversed phase material (Bösger et al., 2009), dried using a Speed-Vac and stored at –
704 80 °C before mass spectrometry analysis. Immediately before LC-ESI-MS/MS, peptides
705 were reconstituted in 25 µL of 5% MeCN/0.1% TFA by vortexing thrice and a 5 min cycle
706 of ultrasonic bath sonication. The samples were then centrifuged for 5 min at 13,000 rpm
707 and the supernatant was transferred to MS vials for LC-MS/MS measurements.
708

709 **Preparation of samples for the secretome proteome**

710 Secretome analysis was performed using cultures grown at 18 °C and 28 °C. Cells were
711 cultivated for four days in TAP medium, as described above. Three independent biological
712 replicates were prepared for each temperature condition. On day 4, cultures were
713 harvested to collect cell-free supernatants. For each sample, the culture was centrifuged
714 at 1,000 *g* for 10 min to remove intact cells and large particulates. The resulting
715 supernatant was then filtered through a 0.22 µm pore-size membrane filter (Carl Roth,
716 Germany) to ensure complete removal of any residual cells or debris.

717 10 mL of the supernatant from each sample were first concentrated to 250 µL using
718 a 3 kDa MWCO Amicon centrifugal filter. Each concentrate was transferred into an
719 Eppendorf Protein LoBind tube and adjusted to 15 µg total protein, as determined by BCA
720 assay. The samples were finally brought to 250 µL with 1 M triethyl ammonium
721 bicarbonate (TEAB) buffer, yielding a final concentration of 50 mM TEAB (pH ~8.5), and
722 incubated at 60 °C for 10 min with shaking at 1,000 rpm.

723 The subsequent steps were performed at 22 °C with shaking at 1,500 rpm. Proteins
724 were sequentially reduced by adding 2.5 µL TCEP to a final concentration of 5 mM and
725 incubated for 10 min, then alkylated with 5 µL iodoacetamide to a final concentration of
726 10 mM for 30 min and finally quenched by adding 5 µL DTT to a final concentration of
727 10 mM for 15 min. Next, a 1:1 mixture of hydrophobic and hydrophilic Sera-Mag
728 carboxylate coated magnetic beads (50 mg mL^{-1}; 2 mg total; particles E3/E7; Cytiva) were
729 prewashed three times with 100 µL water. After washing, 2.5 µL of the bead suspension
730 was added to each sample, followed by ethanol to a final concentration of 60%. Samples
731 were incubated for 5 min to bind proteins. Beads were bound using a magnetic rack. The
732 supernatant was removed, and the beads were washed three times with 400 µL of 80%
733 ethanol and once with 400 µL of MeCN. After an air-drying step, the beads were
734 resuspended in 50 µL of 50 mM TEAB (pH ~8.5).

735 Proteins on the beads were digested by adding 0.5 µL of recombinant LysC (0.2 µg
736 μL^{-1}, MS grade, Promega V1671) and incubation at 37 °C for 1 h with shaking at
737 1,200 rpm. Subsequently, 0.4 µL of trypsin (0.5 µg μL^{-1}, MS grade, Promega VA9000) was
738 added, and digestion continued overnight at 37 °C with shaking at 1,200 rpm. After
739 digestion, the supernatant was collected into a new Protein LoBind tube. The beads were
740 washed twice with 20 µL of 1% TFA, whereby each wash was incubated for 5 min at 22 °C

741 while shaking at 1,000 rpm. The combined supernatant and wash fractions were acidified
742 with 1 µL of 80% TFA (to pH < 3) and desalted using a 100 µL Pierce C18 Tips (Thermo
743 Fisher 87784). Tips were equilibrated with 100 µL of 50% MeCN/0.1% TFA twice, followed
744 by equilibration with 100 µL of 0.1% TFA twice. Samples were loaded by slowly aspirating
745 and dispensing the solution ten times. Tips were washed twice with 100 µL of 0.1% TFA,
746 and bound peptides were eluted three times with 75 µL of 80% MeCN/0.1% TFA. Eluates
747 were combined, dried in a vacuum concentrator at 35 °C, and stored at –80 °C until
748 analysis. Immediately before LC-ESI-MS/MS, peptides were reconstituted in 25 µL of 5%
749 MeCN/0.1% TFA by vortexing thrice and a 5 min cycle of ultrasonic bath sonication. The
750 samples were then centrifuged for 5 min at 13,000 rpm and the supernatant was
751 transferred to MS vials for LC-MS/MS measurements.
752
753 **LC-ESI-MS/MS measurements**
754 LC-MS/MS analysis was performed with an Ultimate3000 Nano-HPLC system (Thermo
755 Fisher Scientific) coupled to an Orbitrap Fusion Tribrid mass spectrometer (Thermo Fisher
756 Scientific). Samples were analyzed using an Acclaim PepMap 100 C18 trap column
757 (0.075 × 200 mm; Thermo Fisher Scientific) and an Aurora Ultimate XT C18 UHPLC
758 analytical emitter column (0.075 × 250 mm; Ionopticks, Collingwood, Australia) in an
759 EASY Spray source setting with HeatSync Column Heater (Ionopticks, Collingwood,
760 Australia). Each sample was loaded onto the trap column, washed with 0.1% TFA in water,
761 and then transferred to the analytical column. Peptides were separated in a 152-minute
762 run (buffer A: water with 0.1% FA, buffer B: MeCN with 0.1% FA, flowrate: 400 nL/min)
763 with the following gradient: from 5% B to 22% B in 105 min, from 22% B to 32% B in 10
764 min, from 32% B to 90% B in 10 min, hold at 90% B for 10 min, then to 5% B over 0.1
765 min, and hold at 5% B for 10 min. The Orbitrap Fusion Tribrid mass spectrometer was
766 operated in a data-dependent acquisition (DDA) mode with a cycle time of 3 s. Full scan
767 acquisition was performed in the Orbitrap at a resolution of 120,000 in the scan range of
768 300 – 1,500 m/z (AGC target of 50%, maximal injection time of 50 ms). Monoisotopic
769 precursor selection as well as dynamic exclusion (exclusion duration: 60 s) was enabled.
770 Precursors with charge states of 2 – 7 and intensities greater than 5e3 were selected for
771 fragmentation. Isolation was performed in the quadrupole using a window of 1.6 m/z.
772 Fragments were generated using higher-energy collisional dissociation (HCD, normalized

773 collision energy: 30%) and detected in the Ion Trap (scan rate: rapid, mass range: normal,
774 maximal injection time: 35 ms, AGC target: standard).
775
776 **Proteomics data analysis along with label-free quantification**
777 All raw LC–MS/MS data were processed with FragPipe version (v22.0), incorporating
778 MSFragger (v4.1) for peptide identification. We applied the built in LFQ MBR workflow to
779 search against the publicly available Chlamydomonas v6.1 reference proteome database
780 supplemented with common contaminants and decoy sequences
781 (CreinhardtiiCC_4532_707_v6.1.protein_primaryTranscriptOnly.fa). MSFragger
782 performed a closed search using initial precursor and fragment mass tolerances of 0.5 Da,
783 followed by automatic mass recalibration and selection of narrower tolerances. The
784 enzyme was set to strict trypsin, allowing up to two missed cleavages, with peptide lengths
785 constrained to 7–50 residues and masses between 500 and 5,000 Da. Methionine
786 oxidation (+15.9949 Da) and protein N terminal acetylation (+42.0106 Da) were set as
787 variable modifications, while cysteine carbamidomethylation (+57.0215 Da) was fixed.
788 Subsequently, MSBooster, Percolator, and Philosopher were employed to generate deep
789 learning augmented scores, perform PSM rescoring, and estimate false discovery rates.
790 Label-free quantification was then carried out with IonQuant (v1.10.27) under default
791 settings, using a mass tolerance of 10 ppm and a retention time tolerance of 0.4 min. Both,
792 “match between runs” and “MaxLFQ” algorithms were enabled. The “min scans”
793 parameter was set to 3, “min isotopes” was set to 2, and “MaxLFQ min ions” was set to 2.
794 Proteins were considered differentially regulated when they exhibited a $|\log_2$ fold change|
795 ≥ 0.5 and an adjusted P-value < 0.05.
796
797 **Predictions of extracellular proteins**
798 DeepLoc 2.1 (Odum et al., 2024) was used to predict the subcellular localization of
799 identified secreted proteins, with the organism type set to "Plant" to optimize predictions
800 for the Chlorophyte alga Chlamydomonas. DeepLoc 2.1 predicts localization up to ten
801 subcellular compartments: nucleus, cytoplasm, extracellular/secreted, mitochondrion, cell
802 membrane, endoplasmic reticulum, chloroplast, Golgi apparatus, lysosome/vacuole, and

803 peroxisome. Proteins were classified as secreted if they received an "extracellular"
804 prediction with a confidence score > 0.5.
805
806 **Crude extracts and immunoblots**
807 Crude extracts of soluble proteins (Zhao et al., 2004) were used for CRY-DASH1 detection
808 and total protein extracts for CHR1 detection (Vuong et al., 2025). Cells were harvested
809 at LD4. For tubulin and CK1 detection, proteins from the MMA fraction were used.
810 Antibodies against CRY-DASH1 (Rredhi et al., 2021), CHR1 (Vuong et al., 2025) and CK1
811 (Schulze et al., 2013) were used. Antibodies against acetylated tubulin were obtained from
812 Sigma-Aldrich (T7451). Immunoblots were performed as described previously (Vuong et
813 al., 2025). Briefly, proteins were separated by SDS-PAGE and transferred to
814 polyvinylidene difluoride (PVDF) membranes that were stained with Coomassie Brilliant
815 Blue R 250. The following dilutions of primary antibodies were taken: 1:5,000 for anti-
816 CRY-DASH1, 1:1,000 for anti-CHR1, 1:5,000 for CK1 and 1:10,000 for anti-acetylated
817 tubulin (T7451, Sigma-Aldrich). The horseradish peroxidase-conjugated anti-rabbit IgGs
818 (Sigma-Aldrich) were used as the secondary antibody or horseradish peroxidase-
819 conjugated anti-mouse IgGs (Sigma-Aldrich) for acetylated tubulin. Dilutions of the
820 secondary antibody were 1:5,000 (CHR1, CK1), 1:6,666 (CRY-DASH1) and 1:10,000
821 (acetylated tubulin).
822
823 **Determination of flagellar length**
824 Flagellar length was quantified on day 4 and day 7 of cell growth. 2 mL aliquots from the
825 main Chlamydomonas cultures were harvested and centrifuged at 500 *g* for 10 min. Ciliary
826 immunolocalization studies were done according to Zou et al. (2017). Cells were
827 incubated with a primary antibody against acetylated tubulin (Sigma, clone 6-11B-1,
828 mouse monoclonal), followed by a goat anti-mouse secondary antibody conjugated to
829 AlexaFluor 555 (Life Technologies, A32727) at a 1:2,000 dilution. Cilia were visualized
830 using Zeiss Axiophot and Leica Stellaris 8 Fluorescent Microscopes, respectively. Flagella
831 length was measured with ImageJ (version 1.53t, Schneider et al., 2012). Statistical
832 analyses and graphing were conducted in RStudio (v.2024.04.1, Posit team, 2023).
833

834 **Motility analysis**

835 Motility analysis of algal cells was performed using day 4 cultures grown in TAP medium
836 at the different temperatures, whose cell density had been standardized to 5×10^5 cells
837 mL^{-1}. A 120 µL aliquot was transferred onto a sterile glass microscope slide fitted with a
838 Gene Frame adhesive chamber (Thermo Fisher Scientific, catalog no. AB0578). Prior to
839 placing the Gene Frame adhesive chamber, slides were cleaned with ethanol and
840 sterilized under UV light for 15 min. After the sample was added, the chamber was sealed
841 with a coverslip that had also been pre-cleaned with ethanol and UV-sterilized. Live-cell
842 imaging was conducted using a Nikon Ti2 widefield fluorescence microscope under a 4x
843 objective. Temperature control during imaging was achieved using a cooling/heating
844 Incubation Insert P-Set 2000 coupled to a DYNEO DD-310F refrigerated and heating
845 circulator (JULABO GmbH, Germany). The imaging temperature was maintained at either
846 18 °C or 28 °C to match the cultivation conditions of each sample. Time-lapse recordings
847 were acquired at intervals of 200 ms per frame. Image sequences were subsequently
848 imported into ImageJ to perform brightness and contrast correction, background
849 subtraction and image thresholding. This results in a series of binary images in which
850 Chlamydomonas cells can be clearly distinguished from the background. Individual cell
851 trajectories were tracked using the TrackMate plugin, which quantified key motility
852 parameters including turning frequency and swimming speed. The extracted tracking data
853 were then exported for statistical analysis and visualization. Trajectory plots were
854 visualized in RStudio.

855

856 **Gametogenesis and mating ability assay** (Jiang and Stern, 2009)

857 Chlamydomonas vegetative cells of strains CC-125 (mt^+) and CC-124 (mt^-) were first
858 transferred from liquid TAP cultures onto solid TAP agar plates and incubated for 4 days
859 at either 18 °C or 28 °C under a 12 h:12 h LD cycle. Following this, cells were transferred
860 onto N10 agar plates and incubated in the dark at their respective temperatures for three
861 additional days to induce nitrogen starvation and promote pregamete formation. Following
862 this, cells were harvested from the N10 plates and resuspended in 10 mL of sterile distilled
863 water that had been acclimatized to the corresponding temperature. Cell suspensions
864 were transferred to sterile NUNC flasks and placed under continuous intense illumination
865 at 70 µmol m^{-2} s^{-1} for 2–3 h without agitation to induce gamete formation. Following

866 induction, mt^+ and mt^- gametes were adjusted to a final concentration of 2×10^6 cells mL^{-1} using a hemocytometer. 1 mL from each mating type were combined in fresh NUNC flasks and kept under continuous light without shaking to allow mating. Mating efficiency was evaluated 1 h after mixing the gametes. Samples from each flask were collected and counted using a light microscope. Large, fused cells were counted as single units. Mating efficiency was calculated using the formula:

Mating efficiency (%) = $2 \times (1 - N_1 / N_0) \times 100$

In this equation, N_0 represents the number of cells per mL immediately after mixing, and N_1 is the number of cells per mL measured 1 h after incubation (Chiang et al., 1970).

Accession numbers

Transcriptome data from this article can be found under the BioProject PRJNA1306621. Motility videos are deposited to Zenodo under DOI: 10.5281/zenodo.16885208. Proteome data was uploaded to PRIDE PXD067459.

880 **Supplementary Data**

881

882 **Data Set 1:**

883 **Supplementary Figure 1.** Boxplot analysis of cell sizes measured on day 7

884 **Supplementary Figure 2.** Temperature-dependent regulation of transcripts encoding
885 TRP channels

886 **Supplementary Figure 3.** Growth curves of Chlamydomonas mono- and cocultures with
887 *P. protegens* at 23 °C (A) and 33 °C (B)

888 **Supplementary Figure 4.** Quantification of flagellar length in cells grown at different
889 temperatures on day 7

890 **Supplementary Figure 5.** Quantification of α-tubulin and CK1 protein abundance within
891 isolated flagella (second independent replicate)

892 **Supplementary Figure 6.** Cell movements with mean directional change (A) and median
893 swimming speed (second independent replicate)

894 **Supplementary Figure 7.** Mating efficiency at different temperatures (second
895 independent dataset)

896

897 **Data Set 2:**

898 **Supplementary Table 1.** Values for growth kinetics of Chlamydomonas at different
899 ambient temperatures compared to 23 °C

900 **Supplementary Table 2.** Values for cell sizes at different ambient temperatures
901 compared to 18 °C

902 **Supplementary Table 3.** Transcript abundances altered in cells grown at different
903 ambient temperatures

904 **Supplementary Table 4.** Full list of gene ontology (GO) terms

905 **Supplementary Table 5.** List of selected candidates along with the genome model
906 numbers from Figures 2 to 6 and Supplementary Figure 2

907 **Supplementary Table 6.** List of identified proteins identified in the ciliary MMA fractions
908 from cells grown at 18 °C or 28 °C

909 **Supplementary Table 7.** List of identified ciliary MMA proteins present in the ciliary
910 database

Supplementary Table 8. List of temperature-dependent significantly up- and downregulated ciliary proteins

Supplementary Table 9. List of ciliary lengths of cells grown at different ambient temperatures compared to 18 °C

Supplementary Table 10. List of identified secretory proteins from cells grown at 18 °C or 28 °C

Supplementary Table 11. List of identified secretory proteins determined by DeepLoc

Supplementary Table 12. List of temperature-dependent significantly up- and downregulated secretory proteins

Video 1. Motility patterns of Chlamydomonas cells grown at 18 °C

Video 2. Motility patterns of Chlamydomonas cells grown at 28 °C

ACKNOWLEDGMENTS

We thank Eduardo Saluzzo and Valentina Mandini from Innova-tech-agro (Italy) for helpful discussions, and Aurelie Jost from the Microverse Imaging Center for help with the Leica Stellaris 8 Fluorescence Microscope. PS, RJA, CCP, ML and MM received funding from the Deutsche Forschungsgemeinschaft (DFG, German Research Foundation) within the Germany's Excellence Strategy – EXC 2051 – Project ID 390713860. JC was funded by DFG under CRC 1127, Project ID 239748522. CL was supported by a PhD grant of the China Scholarship Council (CSC). ML is grateful for support by the research profile line LIFE of FSU Jena and the Deutsche Forschungsgemeinschaft (DFG, German Research Foundation) via the Emmy-Noether-Program (Project ID 528114058). We thank the Microverse Imaging Center also financed by EXC 2051 for providing microscope facility support for data acquisition.

AUTHOR CONTRIBUTIONS

PS, RJA, ML and MM designed the project, PS, VW, DM, CCP, WL, CL, TV, JC and AZ performed experiments, and all authors contributed to analysis and interpretation of results. PS and MM wrote the paper with input from all coauthors.

REFERENCES

Aiyar, P, Schaeme, D, García-Altares, M, Carrasco Flores, D, Dathe, H, Hertweck, C, Sasso, S and Mittag, M (2017) Antagonistic bacteria disrupt calcium homeostasis and immobilize algal cells. Nature Communications, **8**: 1756

Barolo, L, Commault, AS, Abbriano, RM, Padula, MP, Kim, M, Kuzhiumparambil, U, Ralph, PJ and Pernice, M (2022) Unassembled cell wall proteins form aggregates in the extracellular space of *Chlamydomonas reinhardtii* strain UVM4. Applied Microbiology and Biotechnology, **106**: 4145-4156

Barrett, MR and Koch, AR (1982) Effects of ammonium sulfate and urea on the growth of Chlorophycean algae from rice fields. Journal of Environmental Quality, **11**: 187-191

Bösger, J, Wagner, V, Weisheit, W and Mittag, M (2009) Analysis of flagellar phosphoproteins from *Chlamydomonas reinhardtii*. Eukaryotic Cell, **8**: 922-932

Bösger, J, Wagner, V, Weisheit, W and Mittag, M (2014) Comparative phosphoproteomics to identify targets of the clock-relevant casein kinase 1 in *C. reinhardtii* flagella. Methods in Molecular Biology, **1158**: 187-202

Bray, NL, Pimentel, H, Melsted, P and Pachter, L (2016) Near-optimal probabilistic RNA-seq quantification. Nature Biotechnology, **34**: 525-527

Bunbury, F, Deery, E, Sayer, AP, Bhardwaj, V, Harrison, EL, Warren, MJ and Smith, AG (2022) Exploring the onset of B_{12}-based mutualisms using a recently evolved Chlamydomonas auxotroph and B_{12}-producing bacteria. Environmental Microbiology **24:** 3134-3147

Burgunter-Delamare, B, Shetty, P, Vuong, T and Mittag, M (2024) Exchange or eliminate: The secrets of algal-bacterial relationships. Plants, **13**: 829

Carrasco Flores, D, Hotter V, Vuong T, Hou Y, Bando Y, Scherlach K, Burgunter-Delamare B, Hermenau R, Komor AJ, Aiyar P *et al*. (2024) A mutualistic bacterium rescues a green alga from an antagonist. Proceedings of the National Academy of Sciences USA, **121**: e2401632121

Chen, S, Zhou, Y, Chen, Y and Gu, J (2018) fastp: an ultra-fast all-in-one FASTQ preprocessor. Bioinformatics, **34**: i884-i890

Chiang, KS, Kates, JR, Jones, RF and Sueoka, N (1970) On the formation of a homogeneous zygotic population in *Chlamydomonas reinhardtii*. Developmental Biology, **22**: 655-669

Chin, KJ, Lukow, T and Conrad, R (1999) Effect of temperature on structure and function of the methanogenic archaeal community in an anoxic rice field soil. Applied and Environmental Microbiology, **65**: 2341-2349

Christie, JM and Zurbriggen, MD (2021) Optogenetics in plants. New Phytologist, **229**: 3108-3115

Craig, RJ, Gallaher, SD., Shu, S, Salomé, PA, Jenkins, JW, Blaby-Haas, CE, Purvine, SO, O'Donnell, S, Barry, K, Grimwood, J, et al. (2023) The Chlamydomonas

982 Genome Project, version 6: Reference assemblies for mating-type plus and minus
983 strains reveal extensive structural mutation in the laboratory. The Plant Cell, **35**: 644-
984 672
985 **Crockett, C (**2021) How a microorganism corkscrews while it breaststrokes. Physics **14:**
986 s21
987 **Crozet, P, Navarro, FJ, Willmund, F, Mehrshahi, P, Bakowski, K, Lauersen, KJ, Pérez-**
988 **Pérez, ME, Auroy, P, Gorchs Rovira, A, Sauret-Gueto, S and Niemeyer, J,** (2018)
989 Birth of a photosynthetic chassis: a MoClo toolkit enabling synthetic biology in the
990 microalga Chlamydomonas reinhardtii. ACS Synthetic Biology, **7**: 2074-2086
991 **Deisseroth, K and Hegemann, P** (2017) The form and function of channelrhodopsin.
992 Science, **357**: eaan5544
993 **Dupuis, S and Merchant, SS** (2023) *Chlamydomonas reinhardtii*: A model for
994 photosynthesis and so much more. Nature Methods, **20**: 1441-1442
995 **Ermilova, E** (2020) Cold stress response: an overview in Chlamydomonas. Frontiers in
996 Plant Science, **11**: 569437
997 **Folcik, AM, Cutshaw, K, Haire, T, Goode, J, Shah, P, Zaidi, F, Richardson, B and**
998 **Palmer, A** (2020) Quorum sensing behavior in the model unicellular eukaryote
999 *Chlamydomonas reinhardtii*. iScience **23:** e101835
1000 **García-García, A, Cuesta-Valero, FJ, Miralles, DG, Mahecha, MD, Quaas, J,**
1001 **Reichstein, M, Zscheischler, J and Peng, J** (2023) Soil heat extremes can outpace
1002 air temperature extremes. Nature Climate Change, **13**: 1237-1241
1003 **Ghasemi Y, Rasoul-Amini S, Morowvat MH, Raee MJ, Ghoshoon MB, Nouri F,**
1004 **Negintaji N, Parvizi R, Mosavi-Azam SB.** (2008) Characterization of hydrocortisone
1005 biometabolites and 18S rRNA gene in *Chlamydomonas reinhardtii* cultures. Molecules,
1006 **13**: 2416-2425
1007 **Greiner, A, Kelterborn, S, Evers, H, Kreimer, G, Sizova, I and Hegemann, P** (2017)
1008 Targeting of photoreceptor genes in *Chlamydomonas reinhardtii* via zinc-finger
1009 nucleases and CRISPR/Cas9. The Plant Cell, **29**: 2498-2518
1010 **Hallmann, A** (2006) The pherophorins: common, versatile building blocks in the evolution
1011 of extracellular matrix architecture in Volvocales. Plant Journal, **45**: 292-307
1012 **Harris, EH** (1989) The Chlamydomonas sourcebook: a comprehensive guide to biology
1013 and laboratory use. Academic Press, Cambridge
1014 **Helliwell, K.E., Collins, S., Kazamia, E., Purton, S., Wheeler, G.L., and Smith, A.G.**
1015 **(2015)** Fundamental shift in vitamin B_{12} eco-physiology of a model alga demonstrated
1016 by experimental evolution. ISME J. **9:** 1446-1455.
1017 **Hey, S and Linder, S** (2024) Matrix metalloproteinases at a glance. Journal of Cell
1018 Science, **137**: jcs261898
1019 **Hou, Y, Bando, Y., Carrasco Flores, D., Hotter, V., Das, R., Schiweck, B., Melzer, T.,**
1020 **Arndt, H.D. and Mittag, M** (2023) A cyclic lipopeptide produced by an antagonistic
1021 bacterium relies on its tail and transient receptor potential-type Ca^{2+} channels to
1022 immobilize a green alga. New Phytologist, **237**: 1620-1635

1023 **Hughes, CS, Moggridge, S, Müller, T, Sorensen, PH, Morin, GB and Krijgsveld, J**
1024 **(**2019) Single-pot, solid-phase-enhanced sample preparation for proteomics
1025 experiments. Nature Protocols, **14**: 68-85
1026 **Jiang, X and Stern, D** (2009) Mating and tetrad separation of *Chlamydomonas reinhardtii*
1027 for genetic analysis. Journal of Visualized Experiments, **30**: 1274
1028 **Katoh, Y, Terada, M, Nishijima, Y, Takei, R, Nozaki, S, Hamada, H and Nakayama, K**
1029 (2016) Overall architecture of the intraflagellar transport (IFT)-B complex containing
1030 Cluap1/IFT38 as an essential component of the IFT-B peripheral subcomplex. Journal
1031 of Biological Chemistry, **291**: 10962-10975
1032 **Kinoshita, T, Fukuzawa, H, Shimada, T, Saito, T and Matsuda, Y** (1992) Primary
1033 structure and expression of a gamete lytic enzyme in *Chlamydomonas reinhardtii*:
1034 similarity of functional domains to matrix metalloproteases. Proceedings of the
1035 National Academy of Sciences, **89**: 4693-4697
1036 **Lacey, SE, Graziadei, A and Pigino, G** (2024) Extensive structural rearrangement of
1037 intraflagellar transport trains underpins bidirectional cargo transport. Cell, **187**: 4621-
1038 4636
1039 **Lechtreck, KF, Johnson, EC, Sakai, T, Cochran, D, Ballif, BA, Rush, J, Pazour, GJ,**
1040 **Ikebe, M and Witman, GB** (2009) The *Chlamydomonas reinhardtii* BBSome is an IFT
1041 cargo required for export of specific signaling proteins from flagella. Journal of Cell
1042 Biology, **187**: 1117-1132
1043 **Légeret, B, Schulz-Raffelt, M, Nguyen, HM, Auroy, P, Beisson, F, Peltier, G, Blanc, G,**
1044 **Li-Beisson, Y** (2016) Lipidomic and transcriptomic analyses of *Chlamydomonas*
1045 *reinhardtii* under heat stress unveil a direct route for the conversion of membrane lipids
1046 into storage lipids. Plant, Cell & Environment, **39**: 834-847
1047 **L'Hernault, SW and Rosenbaum, JL** (1985) Chlamydomonas α-tubulin is
1048 posttranslationally modified by acetylation on the ε-amino group of a lysine.
1049 Biochemistry, **24**: 473-478
1050 **Li, W, Flores, DC, Füßel, J, Euteneuer, J, Dathe, H, Zou, Y, Weisheit, W, Wagner, V,**
1051 **Petersen, J and Mittag, M** (2018) A musashi splice variant and its interaction partners
1052 influence temperature acclimation in Chlamydomonas. Plant Physiology, **178**: 1489-
1053 1506
1054 **Li, X, Patena, W., Fauser, F., Jinkerson, R. E., Saroussi, S., Meyer, M. T., Ivanova, N.,**
1055 **Robertson, J. M., Yue, R., Zhang, R., et al.** (2019) A genome-wide algal mutant library
1056 and functional screen identifies genes required for eukaryotic photosynthesis. Nature
1057 Genetics, **51**: 627-635
1058 **Lin, CS, Chou, TL and Wu, JT** (2013) Biodiversity of soil algae in the farmlands of mid-
1059 Taiwan. Botanical Studies, **54**: 1-12
1060 **Liu, P and Lechtreck, KF** (2018) The Bardet–Biedl syndrome protein complex is an
1061 adapter expanding the cargo range of intraflagellar transport trains for ciliary export.
1062 Proceedings of the National Academy of Sciences, **115**: E934-E943

1063 **Love, MI, Huber, W and Anders, S** (2014) Moderated estimation of fold change and
1064 dispersion for RNA-seq data with DESeq2. Genome Biology, **15**: 1-21
1065 **Luxmi, R, Blaby-Haas, C, Kumar, D, Rauniyar, N, King, SM, Mains, RE and Eipper,**
1066 **BA** (2018) Proteases shape the Chlamydomonas secretome: comparison to classical
1067 neuropeptide processing machinery. Proteomes, **6**: 36
1068 **Ma, Y, He, J, Li, S, Yao, D, Huang, C, Wu, J and Lei, M** (2023) Structural insight into the
1069 intraflagellar transport complex IFT-A and its assembly in the anterograde IFT train.
1070 Nature Communications, **14**: 1506
1071 **Mäkinen, J, Ellis, EE, Antão, LH, Davrinche, A, Laine, AL, Saastamoinen, M,**
1072 **Conenna, I, Hällfors, M, Santangeli, A, Kaarlejärvi, E, Heliölä, J et al.** (2025)
1073 Thermal homogenization of boreal communities in response to climate warming. Proc
1074 Natl Acad Sci USA, **122:** e2415260122**.**
1075 **Marshall, WF** (2024) Chlamydomonas as a model system to study cilia and flagella using
1076 genetics, biochemistry, and microscopy. Frontiers in Cell and Developmental Biology,
1077 **12**: 1412641
1078 **Marshall, WF and Rosenbaum, JL** (2001) Intraflagellar transport balances continuous
1079 turnover of outer doublet microtubules: implications for flagellar length control. Journal
1080 of Cell Biology, **155**: 405-414
1081 **McCafferty, CL, Papoulas, O, Jordan, MA, Hoogerbrugge, G, Nichols, C, Pigino, G,**
1082 **Taylor, DW, Wallingford, JB and Marcotte, EM** (2022) Integrative modeling reveals
1083 the molecular architecture of the intraflagellar transport A (IFT-A) complex. Elife, **11**:
1084 e81977
1085 **McGoldrick, LL, Singh, AK, Demirkhanyan, L, Lin, TY, Casner, RG, Zakharian, E and**
1086 **Sobolevsky, AI** (2019) Structure of the thermo-sensitive TRP channel TRP1 from the
1087 alga *Chlamydomonas reinhardtii*. Nature Communications **10:** 4180
1088 **Meier, HS, Schuman, IJ, Layden, TJ, Ritz, A, Kremer, CT and Fey, SB** (2022)
1089 Temperature-mediated transgenerational plasticity influences movement behaviour in
1090 the green algae *Chlamydomonas reinhardtii*. Functional Ecology, **36**: 2969-2982
1091 **Merchant, S. S., Prochnik, S. E., Vallon, O., Harris, E. H., Karpowicz, S. J., Witman,**
1092 **G. B., Terry, A., Salamov, A., Fritz-Laylin, L. K., Maréchal-Drouard, et al.** (2007)
1093 The Chlamydomonas genome reveals the evolution of key animal and plant functions.
1094 Science, **318**: 245-250
1095 **Mitchell, BF, Pedersen, LB, Feely, M, Rosenbaum, JL and Mitchell, DR** (2005) ATP
1096 production in *Chlamydomonas reinhardtii* flagella by glycolytic enzymes. Molecular
1097 Biology of the Cell, **16**: 4509-4518
1098 **Moparthi, L, Sinica, V, Moparthi, VK, Kreir, M, Vignane, T, Filipovic, MR, Vlachova, V**
1099 **and Zygmunt, PM** (2022) The human TRPA1 intrinsic cold and heat sensitivity
1100 involves separate channel structures beyond the N-ARD domain. Nature
1101 Communications **13:** 6113

1102 **Müller, N, Wenzel, S, Zou, Y, Künzel, S, Sasso, S, Weiß, D, Prager, K, Grossman, A,**
1103 **Kottke, T and Mittag, M** (2017) A plant cryptochrome controls key features of the
1104 Chlamydomonas circadian clock and its life cycle. Plant Physiology, **174**: 185-201
1105 **Murakami, H, Nobusawa, T, Hori, K, Shimojima, M and Ohta, H** (2018) Betaine lipid is
1106 crucial for adapting to low temperature and phosphate deficiency in *Nannochloropsis*.
1107 Plant Physiology **177:** 181-193
1108 **Odum, M.T., Teufel, F., Thumuluri, V., Almagro Armenteros, J.J., Johansen, A.R.,**
1109 **Winther, O., and Nielsen, H.** (2024). DeepLoc 2.1: multi-label membrane protein type
1110 prediction using protein language models. Nucleic Acids Res. **52:** W215-W220.
1111 **Pan, J and Snell, WJ** (2005) Chlamydomonas shortens its flagella by activating axonemal
1112 disassembly, stimulating IFT particle trafficking, and blocking anterograde cargo
1113 loading. Developmental Cell, **9**: 431-438
1114 **Patel, MB, Griffin, PJ, Olson, SF, Dai, J, Hou, Y, Malik, T, Das, P, Zhang, G, Zhao, W,**
1115 **Witman, GB and Lechtreck, KF,** (2024) Distribution and bulk flow analyses of the
1116 intraflagellar transport (IFT) motor kinesin-2 support an "on-demand" model for
1117 Chlamydomonas ciliary length control. Cytoskeleton, **81**: 586-604
1118 **Pazour, GJ, Agrin, N, Leszyk, J and Witman, GB** (2005) Proteomic analysis of a
1119 eukaryotic cilium. Journal of Cell Biology, **170**: 103-113
1120 **Pedersen LB, Geimer S, Rosenbaum JL (2006)** Dissecting the molecular mechanisms
1121 of intraflagellar transport in Chlamydomonas. Current Biology **16:** 450-459
1122 **Riekhof, WR, Sears, BB and Benning, C** (2005) Annotation of genes involved in
1123 glycerolipid biosynthesis in *Chlamydomonas reinhardtii*: discovery of the betaine lipid
1124 synthase BTA1Cr. Eukaryotic Cell **4:** 242-252
1125 **Rredhi A, Petersen J, Wagner V, Vuong T, Li W, Li W, Schrader L, Mittag M** (2024)
1126 The UV-A receptor CRY-DASH1 up- and downregulates proteins involved in different
1127 plastidial pathways. Journal of Molecular Biology, **436**: 168271
1128 **Rredhi, A, Petersen, J, Schubert, M, Li, W, Oldemeyer, S, Li, W, Westermann, M,**
1129 **Wagner, V, Kottke, T and Mittag, M** (2021) DASH cryptochrome 1, a UV-A receptor,
1130 balances the photosynthetic machinery of *Chlamydomonas reinhardtii*. New
1131 Phytologist, **232**: 610-624
1132 **Salomon, S, Schilling, M, Albrieux, C, Si Larbi, G, Jouneau, PH, Roy, S, Falconet, D,**
1133 **Michaud, M and Jouhet, J** (2025) Betaine lipids overproduced in seed plants are not
1134 imported into plastid membranes and promote endomembrane expansion. Journal of
1135 Experimental Botany **76:** 980-996
1136 **Sasso, S, Stibor, H, Mittag, M and Grossman, AR** (2018) The natural history of model
1137 organisms from molecular manipulation of domesticated *Chlamydomonas reinhardtii*
1138 to survival in nature. eLife, **7**: e39233
1139 **Scaife, MA and Smith, AG** (2016) Towards developing algal synthetic biology.
1140 Biochemical Society Transactions, **44**: 716-722
1141 **Schmidt, M, Geßner, G, Luff, M, Heiland, I, Wagner, V, Kaminski, M, Geimer, S,**
1142 **Eitzinger, N, Reißenweber, T, Voytsekh, O and Fiedler, M** (2006) Proteomic analysis

1143 of the eyespot of *Chlamydomonas reinhardtii* provides novel insights into its
1144 components and tactic movements. The Plant Cell, **18**: 1908-1930
1145 **Schneider, CA, Rasband, WS and Eliceiri, KW** (2012) NIH Image to ImageJ: 25 years
1146 of image analysis. Nature Methods, **9**: 671-675
1147 **Schroda, M, Hemme, D and Mühlhaus, T** (2015) The Chlamydomonas heat stress
1148 response. The Plant Journal, **82**: 466-480
1149 **Schulze, T, Schreiber, S, Iliev, D, Boesger, J, Trippens, J, Kreimer, G and Mittag, M**
1150 (2013) The heme-binding protein SOUL3 of *Chlamydomonas reinhardtii* influences
1151 size and position of the eyespot. Molecular Plant, **6**: 931-944
1152 **Sharma, A, Samtani, H and Laxmi, A** (2024b) Molecular dialogue between light and
1153 temperature signaling in plants: From perception to thermotolerance. Journal of
1154 Experimental Botany, **75**: erae356
1155 **Sharma, S, Sushmita, K, Singh, R, Sanyal, SK and Kateriya, S** (2024a) Phototropin
1156 localization and interactions regulates photophysiological processes in
1157 Chlamydomonas reinhardtii. bioRxiv, doi:10.1101/2024.12.27.630506
1158 **Snell, WJ, Eskue, WA and Buchanan, MJ** (1989) Regulated secretion of a serine
1159 protease that activates an extracellular matrix-degrading metalloprotease during
1160 fertilization in Chlamydomonas. Journal of Cell Biology, **109**: 1689-1694
1161 **Soneson, C, Love, MI and Robinson, MD** (2015) Differential analyses for RNA-seq:
1162 transcript-level estimates improve gene-level inferences. F1000Research, **4**: 1521
1163 **Szydlowski L, Sorokin A, Vasieva O, Boerner S, Fedorovich V, Goryanin I** (2019).
1164 Evolutionary dynamics of microbial communities in bioelectrochemical systems.
1165 Journal of Computer Science and Systems Biology **13**: 1-9.
1166 **Tuxhorn, J, Daise, T and Dentler, WL** (1998) Regulation of flagellar length in
1167 Chlamydomonas. Cell Motility and the Cytoskeleton, **40**: 133-146
1168 **Valledor, L, Furuhashi, T, Hanak, AM and Weckwerth, W** (2013) Systemic cold stress
1169 adaptation of *Chlamydomonas reinhardtii*. Molecular & Cellular Proteomics, **12**: 2032-
1170 2047
1171 **Verret, F., Wheeler, G., Taylor, A.R., Farnham, G., and Brownlee, C. (2010)** Calcium
1172 channels in photosynthetic eukaryotes: implications for evolution of calcium-based
1173 signalling. New Phytol. **187:** 23-43.
1174 **von der Heyde, EL and Hallmann, A** (2022) Molecular and cellular dynamics of early
1175 embryonic cell divisions in Volvox carteri. The Plant Cell, **34**:1326-1353
1176 **Vuong, T, Shetty, P, Kurtoglu, E, Schultz, C, Schrader, L, Then, P, Petersen, J,**
1177 **Westermann, M, Rredhi, A., Chowdhury, S., Mukherji, R., et al.** (2025)
1178 Metamorphosis of a unicellular green alga in the presence of acetate and a spatially
1179 structured three-dimensional environment. New Phytologist, **245**: 1180-1196
1180 **Wemmer, K, Ludington, W and Marshall, WF** (2020) Testing the role of intraflagellar
1181 transport in flagellar length control using length-altering mutants of Chlamydomonas.
1182 Philosophical Transactions of the Royal Society B, **375**: 20190159

1183 **Xiao, Y., Xin, Y., Shen, K., Yang, M., and Wu, H. (2025).** The roles of transient receptor
1184 potential vanilloid in autoimmune diseases. Autoimmun. Rev. **24:** 103872.
1185 **Zhang, Y, Wolf-Yadlin, A, Ross, PL, Pappin, DJ, Rush, J, Lauffenburger, DA and**
1186 **White, FM** (2005) Time-resolved mass spectrometry of tyrosine phosphorylation sites
1187 in the epidermal growth factor receptor signaling network reveals dynamic modules.
1188 Molecular & Cellular Proteomics, **4**: 1240-1250
1189 **Zhang, N, Mattoon, EM, McHargue, W, Venn, B, Zimmer, D, Pecani, K, Jeong, J,**
1190 **Anderson, CM, Chen, C, Berry, JC, Xia, M** (2022) Systems-wide analysis revealed
1191 shared and unique responses to moderate and acute high temperatures in the green
1192 alga *Chlamydomonas reinhardtii*. Communications Biology, **5**: 460
1193 **Zhang, N, Venn, B, Bailey, CE, Xia, M, Mattoon, EM, Mühlhaus, T and Zhang, R** (2024)
1194 Moderate high temperature is beneficial or detrimental depending on carbon
1195 availability in the green alga *Chlamydomonas reinhardtii*. Journal of Experimental
1196 Botany, **75**: 979-1003
1197 **Zhao, B, Schneid, C, Iliev, D, Schmidt, EM, Wagner, V, Wollnik, F and Mittag, M** (2004)
1198 The circadian RNA-binding protein CHLAMY 1 represents a novel type heteromer of
1199 RNA recognition motif and lysine homology domain-containing subunits. Eukaryotic
1200 Cell, **3**: 815-825
1201 **Zou, Y, Wenzel, S, Müller, N, Prager, K, Jung, EM, Kothe, E, Kottke, T and Mittag, M**
1202 (2017) An animal-like cryptochrome controls the Chlamydomonas sexual cycle. Plant
1203 Physiology, **174**: 1334-1347

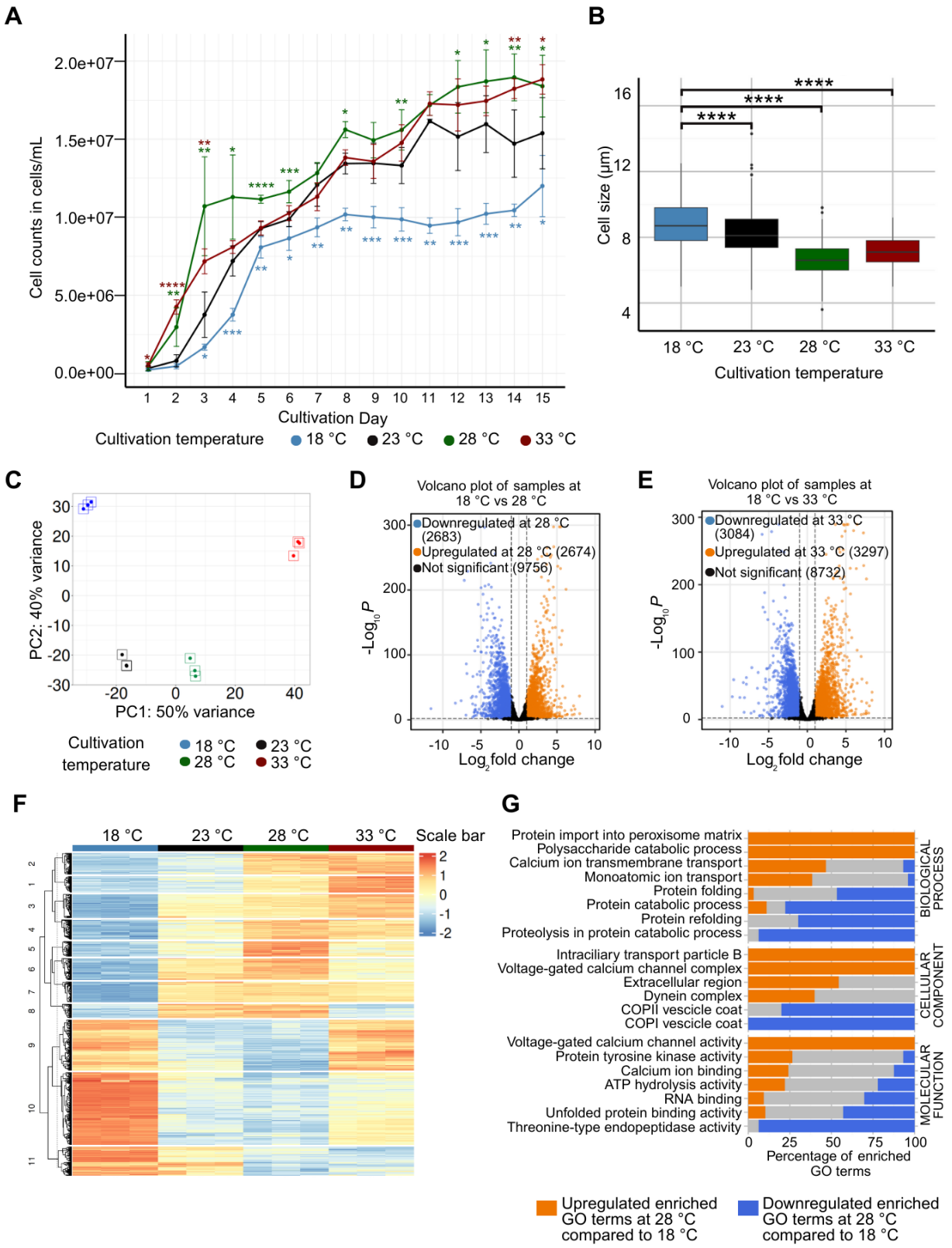

Figure 1: Influence of different ambient cultivation temperatures on the growth and transcript abundances of Chlamydomonas**. A)** Growth curve of Chlamydomonas cultured at 18 °C (blue), 23 °C (black), 28 °C (green), and 33 °C (red) over a 15-day period.

Data points represent mean cell densities (cells mL^{-1}) from two independent replicates, each comprising three biological replicates. Error bars indicate standard deviation. Asterisks indicate the statistically significant differences for 18 °C (black), 28 °C (green), and 33 °C (red) compared to 23 °C as calculated by Student's *t*-test (*: $P < 0.05$, **: $P < 0.01$, ***: $P < 0.001$). **B)** Boxplot of vertical cell size measurements (µm) on day 4 of cultivation across the four temperature treatments. The cell sizes of day 7 are shown in Supplementary Figure 1. Each box represents measurements from three biological replicates (100 cells per replicate). Statistical significance between groups is indicated by asterisks. Asterisks represent significant differences as calculated by Student's *t*-test (****: $P < 0.0001$). **C)** Principal component analysis (PCA) of transcriptomic profiles from Chlamydomonas after 4 days of cultivation at each temperature. Each point corresponds to a biological replicate, colored by temperature (18 °C: blue, 23 °C: black, 28 °C: green, 33 °C: red). PC1 and PC2 account for 50% and 40% of the total variance, respectively, illustrating clear separation by temperature, especially at the extremes. **D–E)** Volcano plots depicting differentially abundant transcripts between 18 °C and 28 °C (D), and 18 °C and 33 °C (E), respectively. Transcripts with significant upregulation (orange) and downregulation (blue) are defined by adjusted *P*-value < 0.01 and $|\mathrm{Log}_2$ fold change$| \geq 1$. Non-significantly changed transcripts are shown in gray. Total transcript counts for each category are indicated in parentheses. Vertical dashed lines mark $\log_2$ fold change thresholds of ±1; the horizontal dashed line marks the significance threshold. **F)** Heatmap showing the expression patterns of the 1,000 most differentially expressed transcripts between 18 °C and 28 °C, clustered across all temperature conditions. Each row represents a gene, and each column a temperature. Transcripts are grouped into clusters based on shared expression patterns, highlighting subsets with temperature-specific regulation. **G)** Exemplary results from a Gene Ontology (GO) enrichment analysis of differentially expressed genes, comparing 18 °C and 28 °C. The full list is shown in Supplementary Table 4. Bar plots display the percentage of enriched GO terms in Biological Process, Cellular Component, and Molecular Function categories. Orange bars indicate GO terms enriched at 28 °C relative to 18 °C, while blue bars represent downregulated terms.

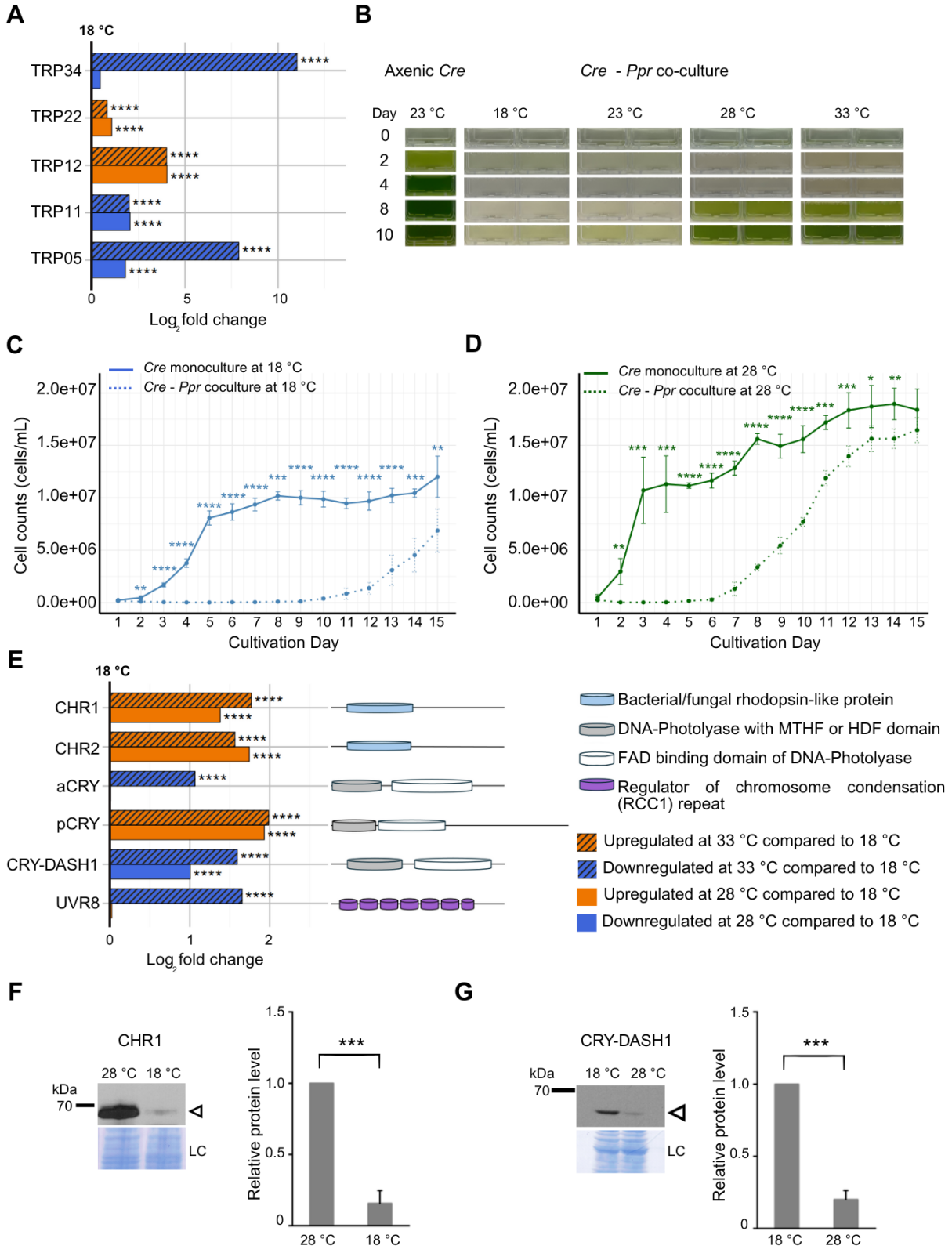

Figure 2: Temperature-dependent regulation of transcripts encoding selected TRP channels and photoreceptors along with mitigation of bacterial antagonism. A) Log_2

fold changes in the expression of selected *TRP* channel transcripts. A list of all significantly changed TRP channel transcripts with a $|\log_2 FC| \geq 1$ in Chlamydomonas in response to cultivation at varying temperatures (18 °C, 28 °C, 33 °C) is presented in Supplementary Figure 2 and Supplementary Table 5. TRPs 5, 11 and 22 are known to be involved in the orfamide A triggered signaling response (Hou et al., 2023). **B)** Visual evidence indicating the attenuation of bacterial antagonism during cocultivation of Chlamydomonas (abbreviated as *Cre*) with *P. protegens* (*Ppr)* at higher temperatures. Green chlorophyll coloration at 28 °C and 33 °C denotes improved algal viability compared to 18 °C, indicating that increased temperature diminishes bacterial antagonistic effects. **C, D)** Growth curves of axenic Chlamydomonas (monocultures) and *Cre–Ppr* cocultures at 18 °C and 28 °C, respectively. Cell densities (cells mL^{-1}) were measured over 15 days, highlighting temperature-associated changes in antagonism. Data points represent mean ± standard deviation cell densities from two independent replicates, each comprising three biological replicates. Statistical significance is indicated by asterisks. **E)** Log_2 fold changes ($|\log_2 FC| \geq 1$) in the expression of photoreceptor transcripts (Supplementary Table 5) under varying temperatures. Known domains of the photoreceptors analyzed by Phytozome 14 (https://phytozome-next.jgi.doe.gov/) are highlighted (Greiner et al., 2017). For simplicity, the size of the proteins has been standardized to a common bar length; the relative position of the domains is given. The bar size for pCRY with more than 1,000 amino acids has been enlarged. CHR, channelrhodopsin; aCRY, animal-like cryptochrome; pCRY, plant cryptochrome; CRY-DASH, *Drosophila Arabidopsis Synechocystis* human cryptochrome. **F)** Immunoblot analysis quantifying CHR1 protein abundances in cells grown at 18 °C and 28 °C. 75 µg of total protein per lane were separated by SDS-PAGE and immunoblotted with the respective antibodies as described in the Methods section. n = 3 biological replicates. Arrows indicate the positions of the target protein. Selected bands from a polyvinylidene difluoride membrane stained with Coomassie Brilliant Blue R250 were used as a loading control (LC). **G)** Immunoblot analysis quantifying CRY-DASH1 under similar conditions as in panel F. In this case, 30 µg of soluble proteins per lane were separated on SDS-PAGE. (**C, D, F, G**) Asterisks represent significant differences as calculated by Student's *t*-test. $P < 0.05$ (*), $P < 0.01$ (**), $P < 0.001$ (***), $P < 0.0001$ (****). (**A, E**) Adjusted *P*-values < 0.00001 (****), as calculated by DESeq2, are shown.

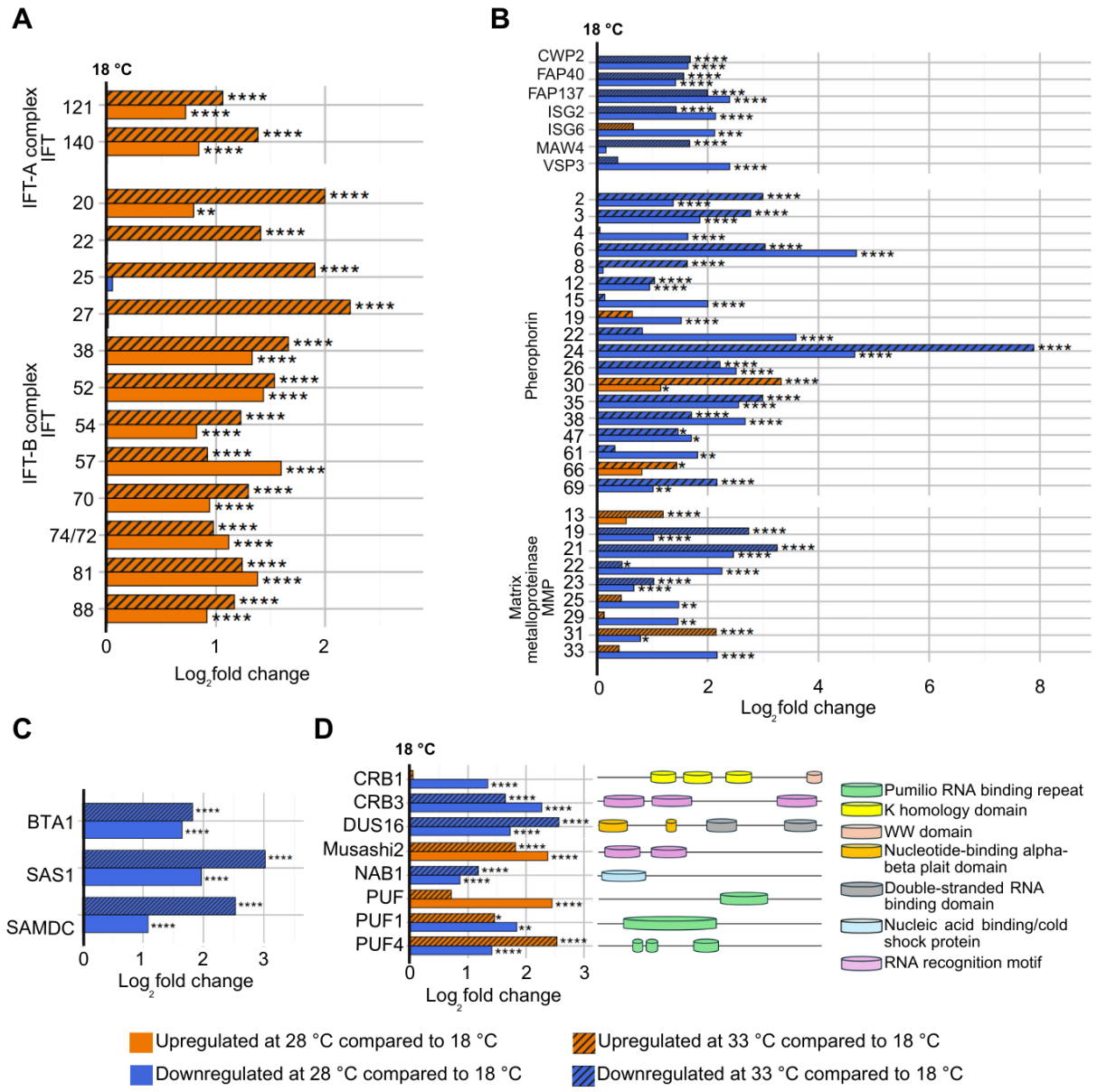

Figure 3: Temperature-dependent regulation of transcripts encoding IFT and extracellular proteins, enzymes of betaine lipid synthesis and RNA-binding proteins. A) Expression of transcripts encoding IFT proteins. Transcripts encoding IFT-A and IFT-B complex with a $|\log_2 FC| \geq 1$ show significantly higher abundance at temperatures of 28 °C and 33 °C. **B)** Expression of transcripts with a $|\log_2 FC| \geq 1$ encoding predicted extracellular proteins as identified by DeepLoc (see Methods) in cells grown at different temperatures. The first seven transcripts encode hydroxyproline-rich glycoproteins. CWP2, cell wall protein2, also known as FAP3; FAP, flagellar associated protein; ISG2/6, inversion-specific glycoprotein, found in cilia; MAW4, membrane associated wall protein; VSP3, serine-proline repeat hydroxyproline-rich cell wall protein found in cilia. **C)** Expression of transcripts with a $|\log_2 FC| \geq 1$ encoding enzymes for betaine lipid biosynthesis. SAS1 (S-adenosylmethionine synthetase1), SAMDC (S-adenosyl-L-methionine decarboxylase), BTA1 (betaine lipid synthase). **D)** Expression profiles of

91 transcripts encoding RNA-binding proteins, including Pumilio/PUF domain proteins,
92 Musashi, CRB1/3 proteins being the C1 and C3 subunit of CHLAMY1, NAB1 (nucleic acid
93 binding factor) and DUS16 (dull slicer-16). Known domains of the RBPs analyzed by
94 Phytozome 14 (https://phytozome-next.jgi.doe.gov/) are highlighted. For simplicity, the
95 size of the proteins has been standardized to a common bar length; the relative position
96 of the domains is given. (**A-E**) Proteins are listed in Supplementary Table 5 along with
97 their Cre accession numbers. Adjusted *P*-values < 0.01 (*), < 0.001 (**) or < 0.0001 (***)
98 or < 0.00001 (****), as calculated by DESeq2, are shown.
99

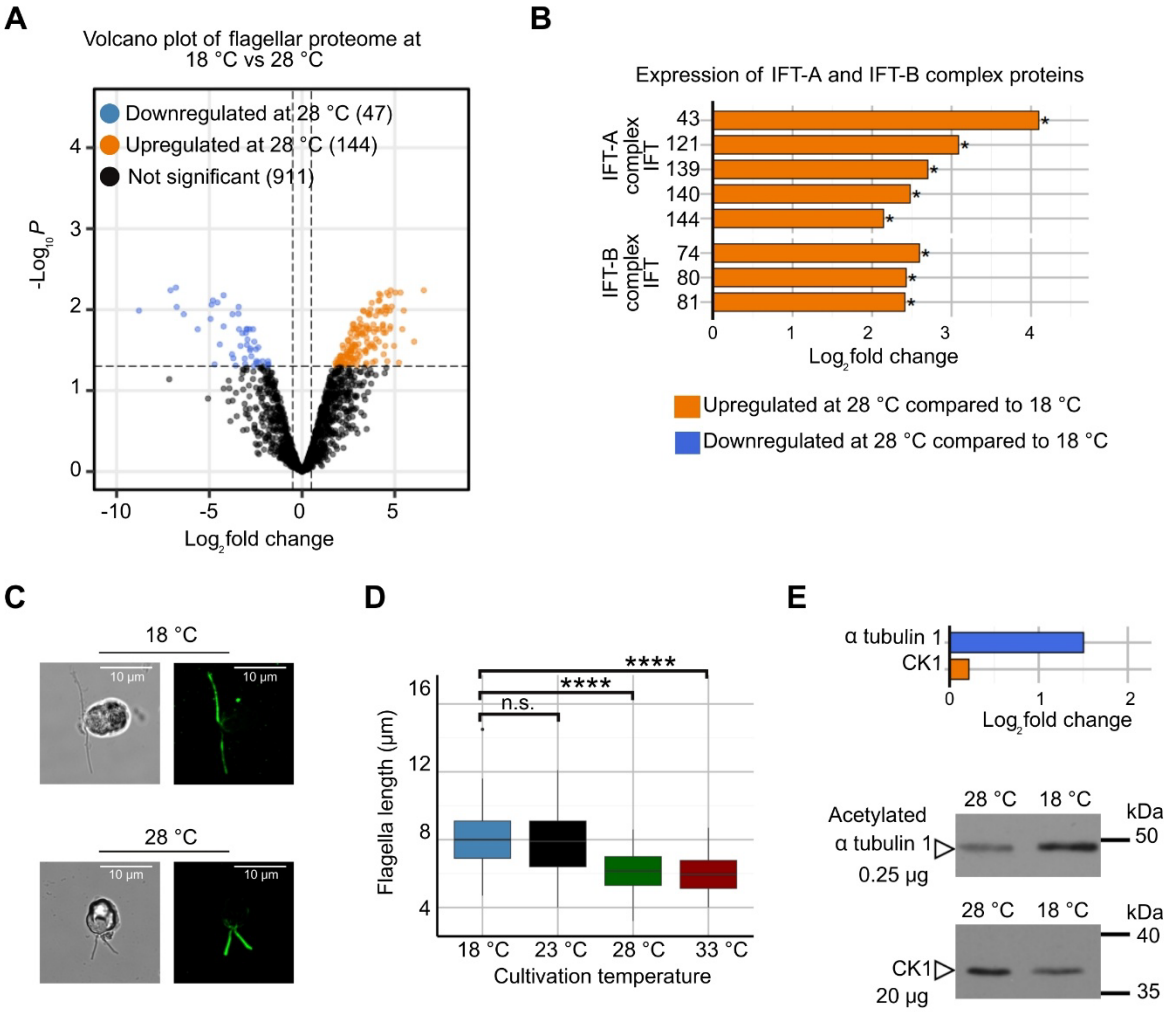

Figure 4: Temperature-dependent remodeling of flagellar proteins alters the length of flagella. A) Volcano plot depicting differentially abundant proteins in the flagellar proteome of Chlamydomonas cultivated at 18 °C and 28 °C. Points represent individual proteins. The orange color indicates proteins upregulated at 28 °C, blue color indicates proteins downregulated at 28 °C, and black represents non-significant changes (adjusted *P*-value < 0.05 and $\log_2$ fold change threshold). Numbers in parentheses denote protein counts per category. Dashed vertical lines indicate ± $\log_2$ fold change of 0.5; the horizontal dashed line marks the significance threshold. **B)** Barplot showing $\log_2$ fold change in IFT-A and IFT-B complex proteins that were significantly differentially abundant in cells grown at 28 °C compared to 18 °C (adjusted *P*-value < 0.05 and $|\log_2$ fold change$| \geq 0.5$). Orange bars indicate upregulation in IFT component abundance, suggesting temperature-dependent modulations in the IFT machinery. **C)** Representative immunolocalization microscopy images of Chlamydomonas cells cultivated at either 18 °C or 28 °C. Left panels show brightfield microscopy images of cells and cilia, right panels depict immunofluorescence images of cilia stained with anti-acetylated tubulin antibodies (see the Methods section). **D)** Quantification of flagellar length in cells grown at 18 °C, 23 °C, 28 °C, and 33 °C on day 4, measured using immunolocalization images. Each boxplot

119 includes measurements from three biological replicates (50 flagella per replicate; n = 150
120 per temperature). Significant differences between temperature treatments were
121 determined by Student's *t*-test and are marked by asterisks (n.s.: not significant; ****:
122 $P < 0.0001$). **E)** Upper panel: Quantification of α-tubulin and CK1 protein abundance within
123 isolated flagella, shown as a barplot from proteome data. Lower panels: As indicated, 0.25
124 µg and 20 µg of proteins per lane from the MMA flagellar fraction isolated from cells grown
125 at 18 °C and 28 °C, respectively, were separated by SDS-PAGE and immunoblotted with
126 (i) anti-acetylated tubulin or (ii) anti-CK1 antibodies as described in the Methods section.
127 An independent biological replicate is shown in Supplementary Figure 5.
128

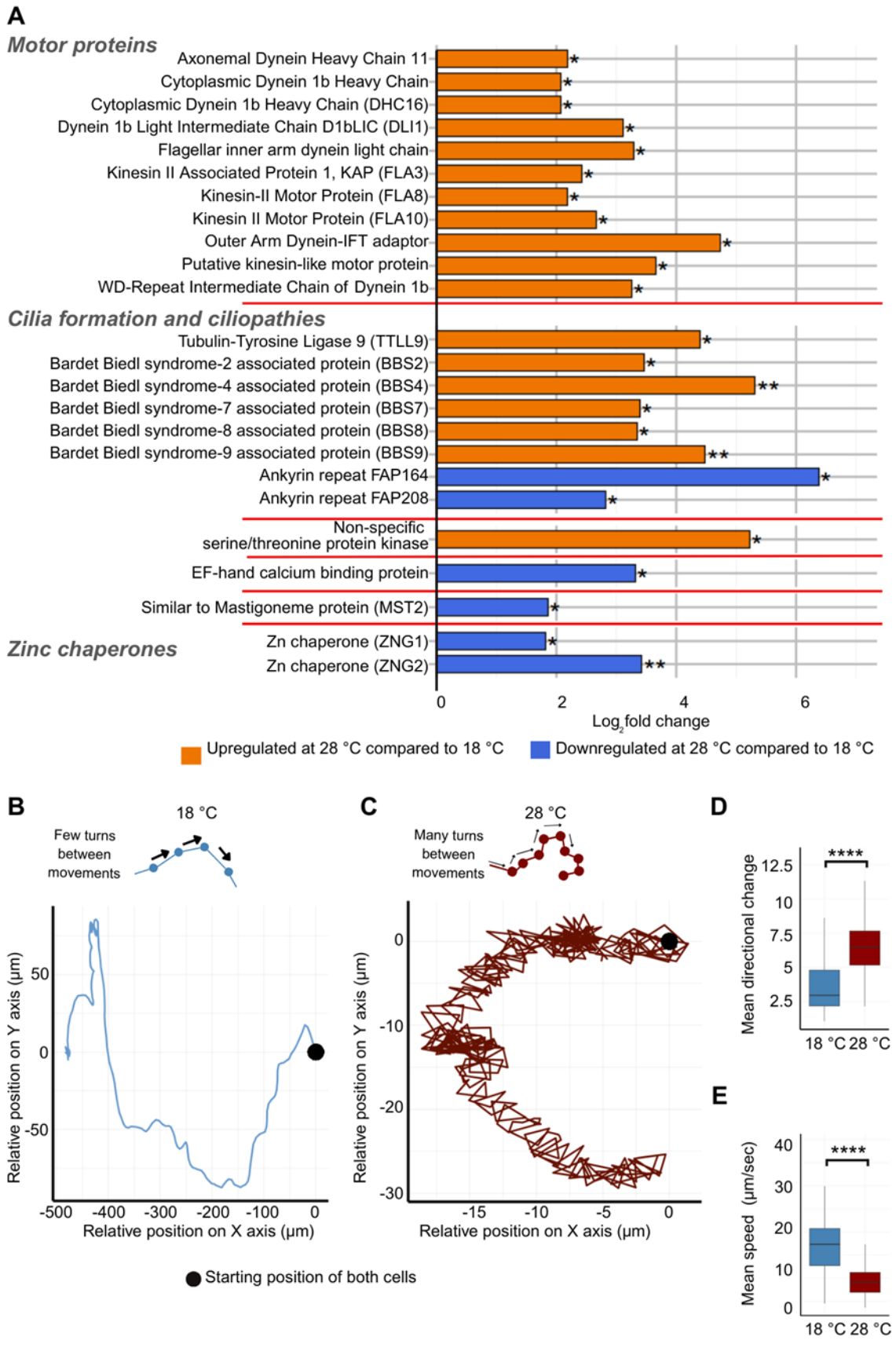
A
Motor proteins
Axonemal Dynein Heavy Chain 11
Cytoplasmic Dynein 1b Heavy Chain
Cytoplasmic Dynein 1b Heavy Chain (DHC16)
Dynein 1b Light Intermediate Chain D1bLIC (DLI1)
Flagellar inner arm dynein light chain
Kinesin II Associated Protein 1, KAP (FLA3)
Kinesin-II Motor Protein (FLA8)
Kinesin II Motor Protein (FLA10)
Outer Arm Dynein-IFT adaptor
Putative kinesin-like motor protein
WD-Repeat Intermediate Chain of Dynein 1b
Cilia formation and ciliopathies
Tubulin-Tyrosine Ligase 9 (TTLL9)
Bardet Biedl syndrome-2 associated protein (BBS2)
Bardet Biedl syndrome-4 associated protein (BBS4)
Bardet Biedl syndrome-7 associated protein (BBS7)
Bardet Biedl syndrome-8 associated protein (BBS8)
Bardet Biedl syndrome-9 associated protein (BBS9)
Ankyrin repeat FAP164
Ankyrin repeat FAP208
Non-specific serine/threonine protein kinase
EF-hand calcium binding protein
Similar to Mastigoneme protein (MST2)
Zinc chaperones
Zn chaperone (ZNG1)
Zn chaperone (ZNG2)
0
2
4
6
Log2 fold change
Upregulated at 28 °C compared to 18 °C
Downregulated at 28 °C compared to 18 °C
B
18 °C
Few turns between movements
Relative position on Y axis (µm)
Relative position on X axis (µm)
C
28 °C
Many turns between movements
Relative position on Y axis (µm)
Relative position on X axis (µm)
Starting position of both cells
D
Mean directional change
****
18 °C 28 °C
E
Mean speed (µm/sec)
****
18 °C 28 °C

129

Figure 5: Remodelling of ciliary proteins and increases in the frequency of algal cell rotations at higher ambient temperature. A) Log_2 fold change of selected flagellar proteins from multiple functional groups in Chlamydomonas compared between cultivation temperatures of 18 °C and 28 °C. Motor proteins (e.g., dyneins, kinesins), ciliopathy-related proteins (BBS proteins, ankyrins), and zinc chaperones display significant upregulation or downregulation, as indicated by colored bars. Orange bars denote proteins upregulated at 28 °C relative to 18 °C, while blue bars indicate downregulation. Statistically significant proteins are marked by asterisks. Adjusted *P*-values < 0.05 (*) and < 0.01 (**) are shown, as calculated by FragPipe. **B-C)** Motility paths tracked for a representative Chlamydomonas cell cultivated either at 18 °C (B) or at 28 °C (C). The first 80 s of the movement are depicted. Please note that the x-axes in B and C show different scales. Cells at 18 °C typically exhibit fewer turns between movements, resulting in relatively straight trajectories. In contrast, cells at 28 °C display frequent directional changes, producing more curved or meandering movement paths compared to 18 °C. **D)** Quantification of mean directional change (degrees) between frames (i.e. at 200 ms intervals) for cells grown at the different temperatures. Data reflects a minimum of 150 individual tracks per temperature per biological replicate, with two biological replicates in total. Statistical significance determined by Student's *t*-test is indicated by asterisks (****: $P < 0.0001$). A second independent biological replicate is shown in Supplementary Figure 6A. **E)** Mean swimming speed (µm/sec) for cells at each temperature, calculated from tracked cell movements. This is calculated by computing the mean swimming speed along each trajectory (in the x-y plane) then averaging this value over trajectories. Data reflects a minimum of 150 individual tracks per temperature per biological replicate, with two biological replicates in total. Statistical significance determined by Student's *t*-test is indicated by asterisks (****: $P < 0.0001$). A second independent biological replicate is shown in Supplementary Figure 6B.

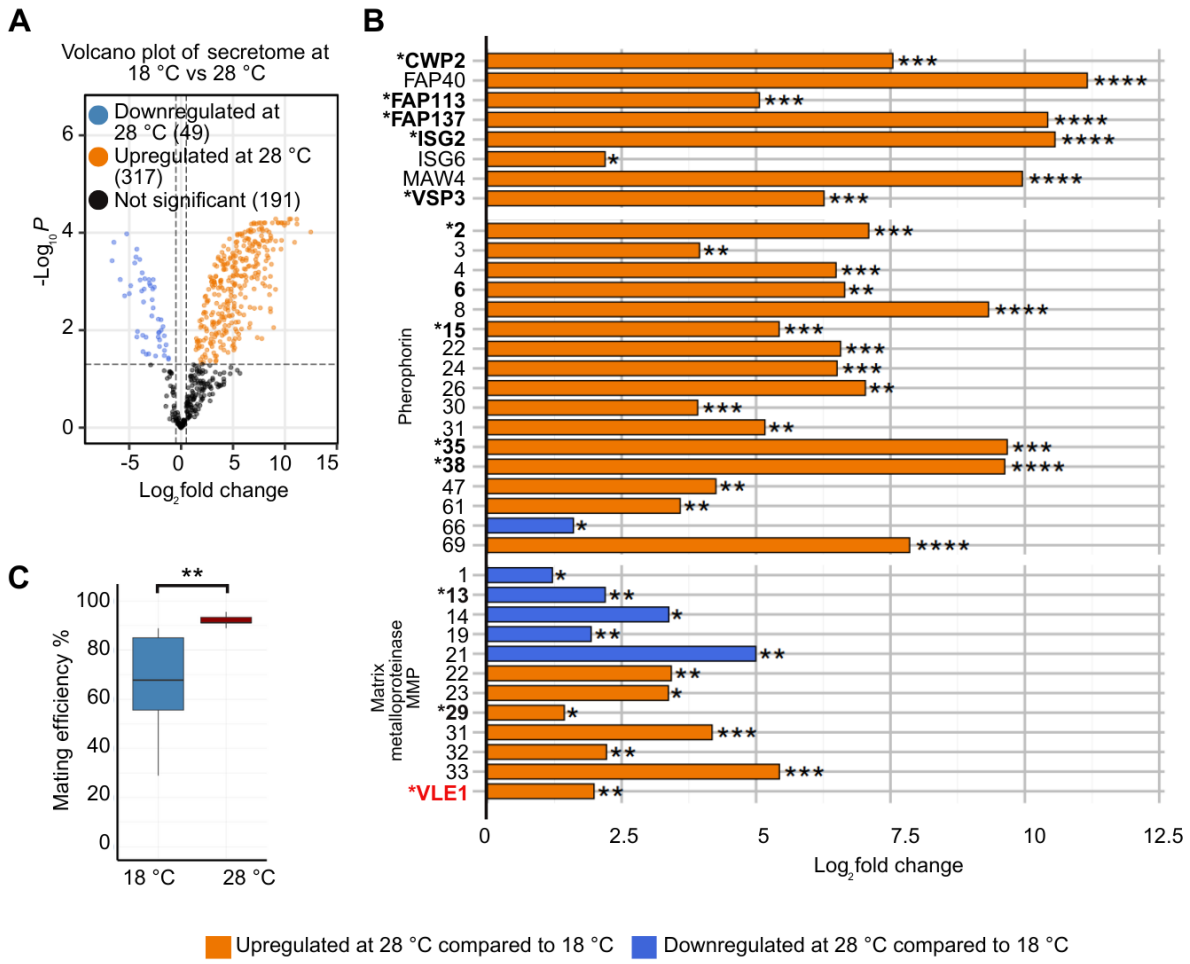

Figure 6: Temperature effects on the secretome, extracellular proteins, and mating efficiency in Chlamydomonas A) Volcano plot depicting differentially abundant proteins in the Chlamydomonas secretome cultivated under 18 °C and 28 °C. Each point represents a unique protein; orange and blue indicate significant up- or downregulation. Axes indicate $\log_2$ fold change versus $-\log_{10}$ (adjusted *P*-value); numbers in parentheses denote protein counts per category. **B)** Barplot showing the $\log_2$ fold changes in abundance of key extracellular proteins as predicted by DeepLoc in the secretome. Notably, the protein VLE1 was detected among soluble mating secretory proteins in previous studies (Luxmi et al., 2018) but was not predicted as extracellular by DeepLoc. Other proteins detected in the soluble mating secretome are highlighted with an asterix and in bold. Adjusted *P*-values < 0.05 (*), < 0.01 (**), < 0.001 (***) and < 0.0001 (****) are shown, as calculated by FragPipe. **C)** Quantification of mating efficiency across temperature or experimental conditions. Data represents three biological replicates. The blots show the proportion of successfully fused mating pairs, with mean values marked. Significant differences in mating efficiency between groups were determined using Student's *t*-test; *P*-values are indicated (**: $P < 0.01$). A second independent dataset with three biological replicates is shown in Supplementary Figure 7.